International Journal of Sustainability and Innovation in Engineering

Editor of Chief

Professor

S. Mehany

THE SCIENCE

PUBLISHING HOUSE

The International Journal of Sustainability and Innovation in Engineering (IJSIE) publishes quality papers that aim to advance engineering science and further education and research in engineering and management. The scope of the journal's topics includes; construction, construction management, controls, electrical engineering and systems, mechanical engineering and systems, structural engineering, and sustainable construction/design in the context of building systems engineering. Subjects include engineering Physics, Chemical Engineering, and bio-engineering. High-quality applied papers outside these sub-disciplines and within engineering will be considered for review. All papers are encouraged to have design or regulatory implications for moving the profession forward. The journal also welcomes papers on engineering education., our publisher is **The Science Publishing House in the USA** www.scipubhouse.com. TSPH is an academic publisher of prestigiously peer-reviewed journals, covering many academic disciplines.

IJSIE

Vol. 1, No. 1. June 2023

THE SCIENCE PUBLISHING HOUSE

Contents

International Journal of Sustainability and Innovation in Engineering (IJSIE)
https://www.doi.org/10.56830/IJSIE062023

Effect of SHEAR SPAN-TO DEPTH RATIO OF Concrete Beams Reinforced with GFRP bars on Shear under Fire Exposure

https://www.doi.org/10.56830/IJSIE06202301

M. A. OSMAN[1], Hala Mamdouh[2], Ahmed H. Ali[3], , and T.S.Kamal[4]

[1] Professor of Civil Engineering, Helwan University, Cairo, Egypt.
E-mail: m_osman62@yahoo.com

[2]*Assoc. Professor of Civil Engineering, Helwan University, Cairo, Egypt.*
E-mail: dr_hala_mamdoh@yahoo.com

[3]*Assistant. Professor of Civil Engineering, Helwan University, Cairo, Egypt*
E-mail: Ahmed.Ali@usherbrooke.ca

[4]Lecturer assistant, Civil Engineering, Helwan University, Cairo, Egypt.
E-mail: taher.sayed030@gmail.com

ABSTRACT:

Glass bars for concrete reinforcement, known as glass fiber-reinforced polymers (GFRPs), are new natural inorganic materials with distinct mechanical properties that have been used recently in the construction field. Generally, the FRPs bars have no yield before the brittle failure as steel bars and their behavior, when exposed to fire, is still under investigation, this paper presents an experimental study to get more knowledge about the characteristics and the fire resistance of a concrete beam reinforced using GFRPs. Three-scale concrete beams were constructed and tested up to failure under direct fire at 500 ◦C for an hour. Shear span-to depth ratio is the main parameter of this study. Beam (B1) had distance from face of support 670 mm ,beam (B2) had distance from face of support 250 mm and beam (B3) had distance from face of support 500 mm .All beams had 30 mm concrete cover , exposed to fire for an hour and three GFRPs reinforcement bars were used. The results are discussed in terms of load capacity, cracking behaviour, and failure modes.

Moreover, the experimental results are compared with theoretical calculations according to the ACI code and other codes. The results show that when distance from face of support over effective depth greater than 2.5 the beams act as slender beams while distance from face of support over effective depth less than 2.5 the beams act as arch action. Our results also showed that when distance from face of support over effective depth 2.02 the failure load incress by percent 60.3% and beam failure as shear failure while distance from face of support over effective depth 1.01 the failure load incress by percent 221.7% and beam failure as flexural failure . More studies are needed to justify our observations in details and determine their applicabilities under different conditions.

1.INTRODUCTION

The development of Fiber Reinforced Polymer (FRP) materials began in the 1940s for military and aerospace applications (Ballinger, 1990) .FRP are be-coming increasingly popular in the engineering applications as alternative to conventional engineering materials. The unique characteristics of FRP such as their light weight, their resistance to corrosion, and the lower cost of construc-tion and maintenance, are very promising in the application of FRP in civil engineering (Lin, 1995). A fiber is a material made into a long filament. According to (Zobel, 2004), a single fiber usually has a diameter up to 15 um. Bigger diameters generally increase the probability of surface defects. The aspect ratio of length and di-ameter can be ranging from thousand to infinity in continuous fibers. They usually occupy 30-70% of the volume of the composite and 50% of its weight. The main functions of fibers are to carry the load and provide stiff-ness, strength, thermal stability and other structural properties to the FRP (Tuakta, 2005). To perform these functions, the fibers in FRP composite must have high modulus of elasticity, high ultimate strength, low variation of strength among fibers, high stability of their strength during handling and high uniformity of diameter and surface dimension among fibers. The type of fibers used as the reinforcement is the basics for classification of FRP composites. There are three types of fibers dominating civil engineering industry: glass, carbon and aramid fibers. The glass fiber strands and woven fabrics are the forms most commonly used in civil engineering application. Relatively low cost compar-ing to other kinds of fibers makes E-glass fibers the most commonly used fi-bers available in the construction industry. The disadvantages of glass fibers are a relatively low young´s modulus, the low humidity and alkaline re-sistance as well as low long term strength due to stress rupture .Six reinforced concrete beams were cast at the Construction TechnologyLaboratories of the Portland Cement Association were tested by Bruce Ellingwood' and T. D. Lin,2 Members [5]. All beams were designed according to ACI Standard 318 {Building 1983). Beams were fabricated using normal-weight concrete (Type I portland cement, sand, and carbonate gravel aggregate) with a specified compressive strength of 4,000 psi (2.8 MPa) and Grade 60 deformed reinforcing bars.They found that thickness of concrete cover has little effect on the deflection of beams during the first 3 hr of the fire if the beams are designed in accordance with ACI Standard 318. (Kodur, Bisby, & Foo, 2005) tested a series of concrete slabs reinforced internally with either steel or FRP reinforcing bars and subjected to a standard fire. Several parameters were varied between the slabs, including the reinforcement type (steel, glass FRP, or carbon FRP), the concrete aggregate type (siliceous or carbonate), the concrete cover thickness, and the overall slab thickness. The slabs were tested under self

weight only and exposed to the (ASTM, 2005) standard fire.He found that The deterioration of bond properties for FRP bars (which has been shown to be much more severe than the bond deterioration of conventional steel reinforcement at elevated temperatures (Katz, Berman, & Bank, 1993) is not well-known and may vary depending on the fibre type, matrix type, any matrix fillers used in the manufacture of the bars, the surface treatment and deformations on the bars, and the presence of bar splices and/or bends. Studying experimentally the effects of using different ratios of steel bars with basalt bars in the same beam at the normal temperature (25 ◦C) and under fire exposure (500 ◦C for 2 h) on the load capacity, crack pattern, and failure type is provided by (Hend, 2021). Eight reinforced concrete beam specimens were tested in this study. The beam specimens were classified into two groups (G1, G2) according to the fire degree. The effect of high temperatures was evident from the continuous decrease in the load capacity of the beams. This decay was relative to the BFRP bar ratio in the reinforced beams as the load capacity of the steel-reinforced beam was more pronounced than those obtained with 33%, 67%, and 100% of BFRP bars. Consequently, the decrease in failure load was 6–23% compared with that of normal beams at 25 ◦C, owing to the lower thermal conductivity of the BFRP bars as well as BFRP bars have almost the same thermal coefficient of expansion as concrete (Subramanian, 2013).

2. Research objective

In this research the chosen rate of fire is (500 ◦C for an hour) as it high enough to represent a fire event, also the concrete has a lower coefficient of thermal conductivity so the movement of heat through it is slow and thus the reinforcement inside it is protected, this rate ensures reaching this temperature to the core of concrete and the internal reinforcement. The main purposes of this research are:

- Studying experimentally the effects of distance from face of support over effective depth ratio under fire exposure (500 ◦C for an hour) on the load capacity, crack pattern, and failure type.
- Theoretical calculations for beam specimens under fire sexposure at 500 ◦C for an hour.
- Throughout this research, the results may provide fundamental information about the performance of beams reinforced using glass bar as a flexural reinforcement and be able to predict their response under fire exposure.

3.Experimental Work

3.1. Materials

Experimental concrete mixes were prepared to yield a design compressive strength (fcu) of 31.19 MPa after 28 days. Concrete was produced by adjusting the size of thin and rough aggregates and increasing the quantity of cement paste to

achieve high workability and reduce the risk of separation during the placing of concrete. After many attempts of producing the concrete mixes, the final ratios of the contents used for the mixing concrete are as shown in Table 1. The components were mixed using a cylinder tilting rotary mixer. The coarse aggregates, fine aggregates, and cement were dry mixed. Subsequently, water was added at regular intervals into the concrete blend after measuring the amount of cement, and the cement–water ratio was 0.5. The concrete mix was blended for two more minutes, resulting in a homogeneous concrete mixture. From the concrete mixture, ten cubes measuring 150 mm × 150 mm × 150 mm were cast to determine the compressive strength. The casting and curing processes were performed according to the procedures stipulated in the ECP standard specification (ECP, 2018); (ECP 2. , 2005) . 12 mm diameter were used as bottom GFRPs reinforcement for all beams. To evaluate the axial tensile strength, at least three samples of bar 12 mm diameter were tested. Electrical strain gauges were bonded at the middle of bar to measure the strain in the bars during the test. As shown in Fig. 1, the test was performed using a Shimadzu machine at the strength of the materials laboratory at Helwan University. The stress-strain curves of the tested bars are shown in Fig. 2. Glass Fiber Reinforced Polymer wrap used in this research was provided by the national center for quality supervision and test of building engineering (BETC-CL2-2014–311(A)).

Table (1) Proportions of Components in Concrete Mixture

Compressive Strength fcu (MPa)	Cement Content (kg/m3)	Fine Aggregates (kg/m3)	Coarse Aggregates (kg/m3)	Water–Cement Ratio
31.19	390	785	1325	0.5

Fig.1.ShimadzuMachine.

International Journal of Sustainability and Innovation in Engineering
(IJSIE)
https://www.doi.org/10.56830/IJSIE062023

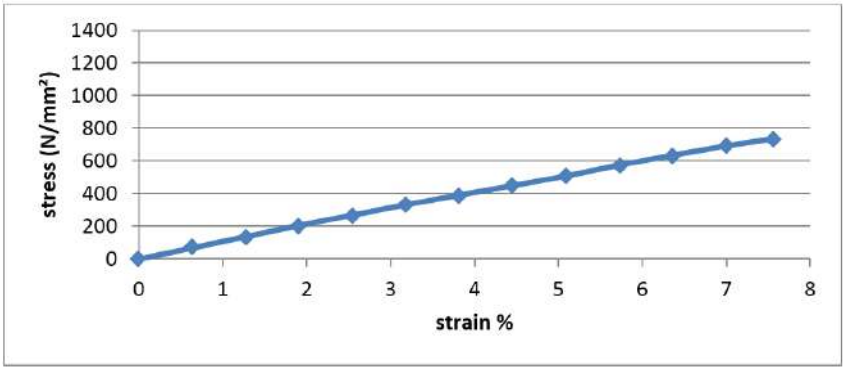

Fig. 2. Stress-Strain Curve for Glass Bar

Table (2) Details of Beam Specimens Prepared in This Study.

Sample name	Fire duration (hour)	Concrete Cover (mm)	d (mm)	a (mm)	a/d (mm)
B1	1	30	248	670	2.70
B2	1	30	248	250	1.01
B3				500	2.02

3.2. Preparing test specimens

Three reinforced concrete beam specimens measuring 150 mm × 300 mm were tested in this study, with a total span of 1650 mm. beams were constructed and tested up to failure under direct fire at 500 ◦C for an hour. Beam (B1) had distance from face of support 670 mm ,beam (B2) had distance from face of support 250 mm and beam (B3) had distance from face of support 500 mm .All beams had 30 mm concrete cover , exposed to fire for an hour and three GFRPs reinforcement bars were used, as shown in Table 2. For the top reinforcement, two 8-mm steel bars for the top reinforcement and three 12-mm GFRPs bars for the bottom reinforcement. The details of the reinforcement and the cross-section of the tested beams are illustrated in Fig. 3. Reinforcement cages were prepared and thirteen clean smooth wooden forms were used for casting all the test specimens as shown in Fig. 4. All beam specimens were cured regularly by a sprinkling of water and covered by sackcloth to prevent moisture release from the concrete surface until the date of testing. Cubes were curing by immersing them in water.

International Journal of Sustainability and Innovation in Engineering
(IJSIE)
https://www.doi.org/10.56830/IJSIE062023

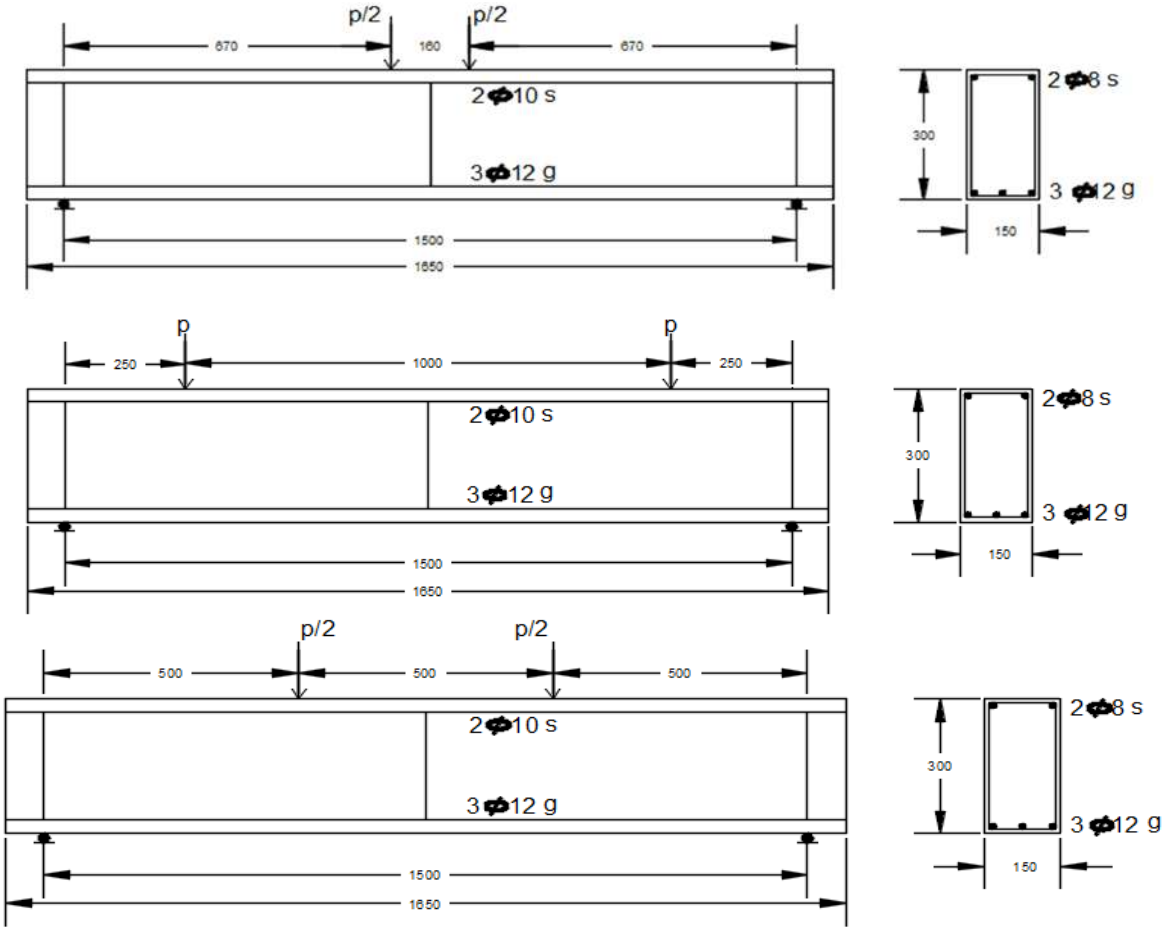

Fig. 3. Details of Tested Beams.

Fig. 4. Details of Reinforcement and Wooden Forms.

International Journal of Sustainability and Innovation in Engineering
(IJSIE)
https://www.doi.org/10.56830/IJSIE062023

Fig. 5. Beams subjected to Fire.

3.3. Fire exposure system

A steel furnace with seven burners lined parallel to each other was used with dimension 2000 mm × 2000 mm × 600 mm; the furnace was heated to the required temperature, i.e. (500 ◦C) and then kept at this temperature for an hour. The beams subjected to direct fire are shown in Fig. 5. The used regime for cooling the fire beams was air.

3.4. Experimental setup and testing

All the beam specimens were subjected to two-point loading under an incremental force control which increased by 2kN per grade until cracks appearing, and then 4kN per grade up to the failure load. During the loading tests, load cells were used to measure the applied load, three linear variable differential transducers (LVDT) were used to measure the deflection (the first one at mid-span, the second under loading point and the third mid between loading point and support, sensors were used to prevent damage during the tests, electrical strain gauges (60 mm length) were attached to measure the concrete strain. The strain gauges were fixed on the at top surfaces of the mid span. The digital load cell of capacity 550kN was adopted to measure the applied load, the load increments, and the displacements were read directly from the data recorder. The crack growth of the specimens during loading and at the time of failure was observed. The test setup and instrumentation are illustrated in Fig. 6.

Fig. 6. Experimental Test Setup, Load Cell, and Data Logger and Reader.

International Journal of Sustainability and Innovation in Engineering
(IJSIE)
https://www.doi.org/10.56830/IJSIE062023

4. Results and discussion

4.1. Cracking load and ultimate load

Table 3 shows the results of all tested beams, including the cracking load and its corresponding deflections (Pcr and Δcr) as well as the ultimate load and its corresponding deflection (Pf and Δf). Furthermore, the failure patterns of the GFRP tested beams were observed. Fig. 7 illustrates the effect a/d ratio on the cracking and ultimate loads for all specimens at 500 ◦C. Overall, the quick glance of Table 3 and Fig. 7 reveal that there is a direct relation between a/d ratio and corresponding load capacity values at 500 ◦C for an hour. Turning to details, when distance from face of support over effective depth greater than 2.5 the beams act as slender beams while distance from face of support over effective depth less than 2.5 the beams act as arch action. Our results also showed that when distance from face of support over effective depth 2.02 the failure load incress by percent 60.3% and beam failure as shear failure while distance from face of support over effective depth 1.01 the failure load incress by percent 221.7% and beam failure as flexural failure.

Table (3) Summarised Results for Beams Reinforced Using GFRP Bars at 500 ◦C.

Sample name	Fire duration (hour)	Concrete Cover (mm)	d (mm)	a (mm)	a/d (mm)	First Crack Stage		Failure Stage		Pf / Pcr	Δf / Δcr	Failure Mode
						Pcr(KN)	Δcr (mm)	Pf (kN)	Δf (mm)			
B1	1	30	248	670	2.70	16.10	0.98	72.30	16.81	4.49	17.20	Shear Failure
B2	1	30	248	250	1.01	17.40	0.74	232.60	15.74	13.37	21.18	Flexural Failure
B3				500	2.02	15.80	1.18	115.90	19.37	7.34	16.49	Shear Failure

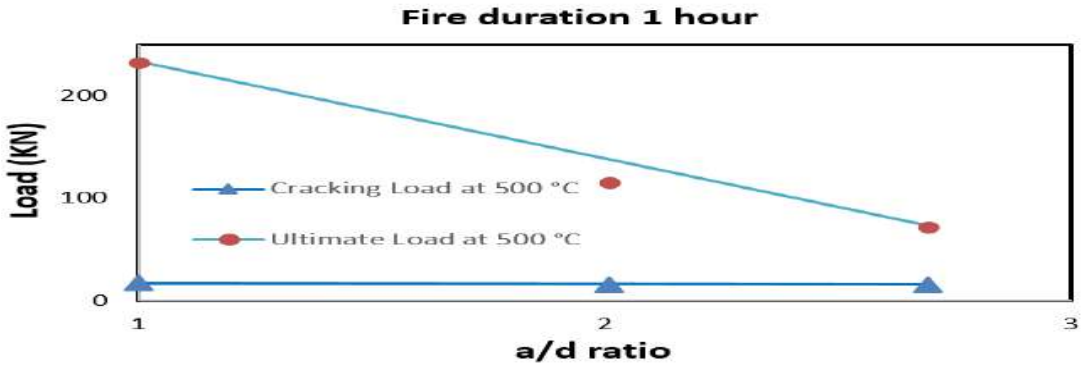

4.2. Crack pattern and failure mode

Fig. 8 shows the crack development and failure type for all tested beams. The crack patterns at both faces of all beams were recorded at several load stages up to failure. Comparing the load patterns at both faces revealed that both patterns are

largely similar. The specimen remained with no visible cracks until flexural cracking took place. Flexural cracking at first took place at mid-span of the tested beams then flexure-shear cracking and flexural cracking extended over the beam. As loading increased, more flexural and diagonal cracks were formed and cracks became wider. As clearly, the failure mode depend on a/d ratio. Due to fire exposure, wider and fewer flexural cracks developed, owing to the reduced strength of concrete and the susceptibility of the resin on the surface of the GFRPs to soften, thereby resulting in a lower bond between reinforcement and surrounding concrete (Hamad, Megat, & Haddad, 2017), concrete in the compression zone crushed and the concrete cover spalled, the concrete spalling behaviour occurs in the condition of fire due to the low permeability of concrete, which limits the ability of water vapor to escape from the pores, this results in inducing internal pore pressure and thermal stresses (Kalifa & Quenard, 2000).

4.3. Load deflection curve

Fig. 9 shows the relationship between the applied load and mid-span deflection for the studied beams, most of the tested beams failed in a ductile manner with large mid-span deflection thus absorbing more energy during failure. The deflections of all beams increased uniformly during loading. As shown, the behaviour of the load–deflection curve of the GFRP reinforced beam was linear before cracking and slightly nonlinear up to failure with lack of yielding. the GFRPs beams with a/d 2.02 the incresse percentage in deflection 15.25%, while the GFRPs beams with a/d 1.01 the incresse percentage in deflection 35.4%. The increased deflection will lead to extensive cracking along the length of the beam, thereby significantly reducing its flexural and shear stiffness. So the stiffness of the GFRP RC beam obviously decreased after cracking.The effect of high temperatures was evident from the continuous decrease in the load capacity of the beams.

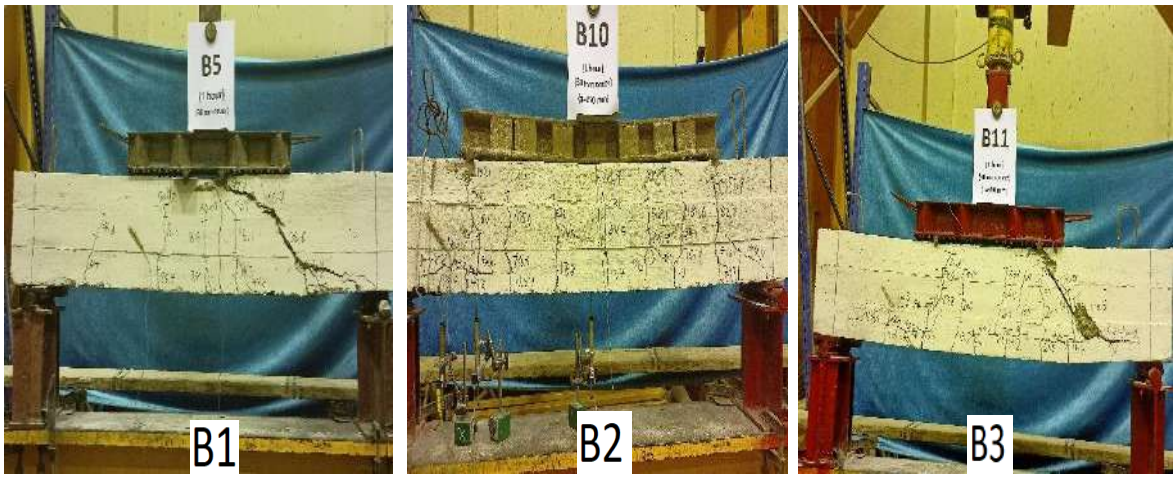

Fig. 8. Crack pattern and Failure Mode of Tested Beams.

International Journal of Sustainability and Innovation in Engineering
(IJSIE)
https://www.doi.org/10.56830/IJSIE062023

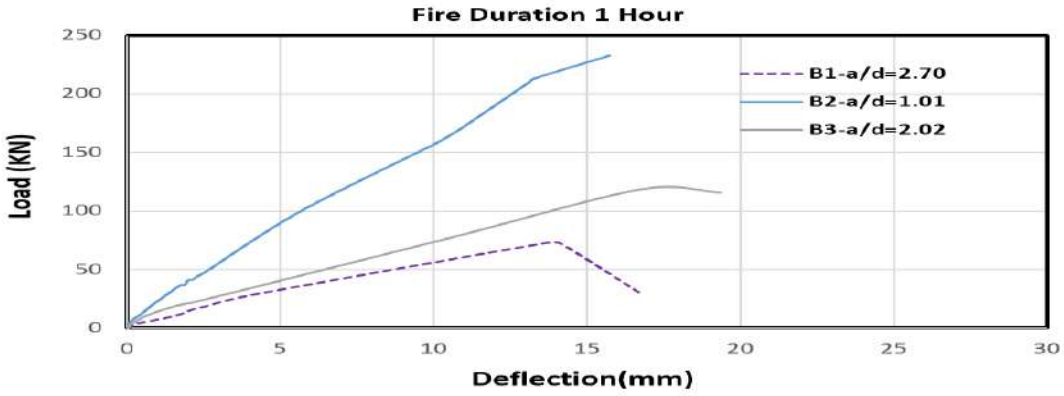

Fig. 9. Load–Deflection Curves at Mid Span for Beams Tested.

4.4. Strain of Concrete

The relation between the concrete at compression zone and the applied load is shown in Figure (10). The strain gauge located at top surfaces of the mid span

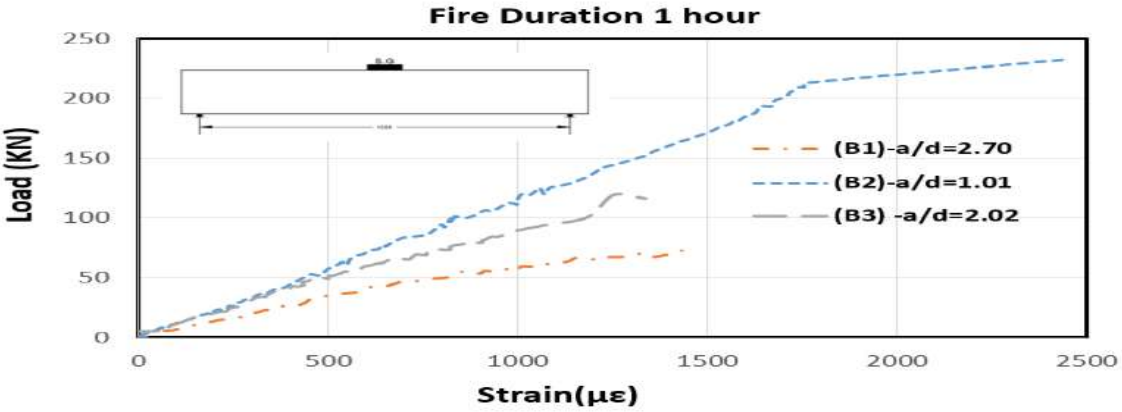

Fig. 10. Load-strain relationship for the concrete at top compression zone.

Conclusions

The conclusions of this study are as follows:

- when shear span-to depth ratio greater than 2.5 the beams act as slender beams while shear span-to depth ratio less than 2.5 the beams act as arch action.
- when shear span-to depth ratio 2.02 the failure load incress by percent 60.3% and beam failure as shear failure while shear span-to depth ratio 1.01 the failure load incress by percent 221.7% and beam failure as flexural failure.
- By controlling shear span-to depth ratio (a/d) ratio, a reasonable deflection and crack width could be achieved and accordingly satisfying serviceability requirements.

- the GFRPs beams with shear span-to depth ratio (a/d) 2.02 the incresse percentage in deflection 15.25%, while the GFRPs beams with shear span-to depth ratio (a/d) 1.01 the incresse percentage in deflection 35.4%

References:

ASTM. (2005). Standard methods of fire test of building construction and materials. ASTM E119-05a, American Society for Testing and Materials. *West Conshohocken, PA*, 22.

Ballinger, C. (1990). "Structural FRP Composites". *ASCE Civil Engineering, vol. 60*, pp. 63-66.

ECP, 2. (2005). Egyptian Code for the Use of Fiber Reinforced Polymers in the Construction Field. *Housing & Building National Research Center, Cairo, Egypt*.

ECP, 2. (2018). Egyptian Code for Design and Construction of Concrete Structures. *Housing and Building National Research Center, Cairo, Egypt*.

Hamad, R., Megat, J. M., & Haddad, R. H. (2017). Haddad RH. Mechanical properties and bond characteristics of different fiber reinforced polymer rebars at elevated temperatures. *Constr Build Mater;142,* 521–535.

Hend, E. (2021). "Behaviour of concrete beams reinforced using basalt and steel bars under fire exposure". *M.Sc.thesis, University of Helwan University, Cairo*.

Kalifa, M. F., & Quenard, D. (2000). Spalling and porepressure in HPC at high temperature. *Cement Concr Res ;1*, 1915–1927.

Katz, A., Berman, N., & Bank, L. (1993). Effect high temperature on the bond strength of FRP rebars. *J Compos Constr, 3(2)*, 73–81.

Kodur, V., Bisby, L., & Foo, S. (2005). Thermal behaviour of fire-exposed concrete slabs reinforced with fibre reinforced polymer bars. *ACI Struct J, 102(6)*, 799–808.

Lin, Z. M. (1995). "Analysis of pole-type structure of fiber-reinforced plastics by finite element method". *Ph. D. thesis, University of Manitoba, Manitoba, Canada*.

Subramanian, N. (2013). Sustainability of RCC Structures Using Basalt Composite Rebar. *Gaithersburg, MD, USA; September*.

Tuakta, C. (2005). Use of Fiber Reinforced Polymer Composite in Bridge Structures,. *Massachusetts Institute of Technology*.

Zobel, H. (2004). Mosty kompozytowe,50. *Jubileuszowa Konferencja Naukowa Kiliw pan i KN PZITB, Krynica,*.

International Journal of Sustainability and Innovation in Engineering
(IJSIE)
https://www.doi.org/10.56830/IJSIE062023

Shear Contribution of GFRP Reinforced Concrete Beams Mixed with Seawater, Freshwater, and Chopped Glass Fiber

https://www.doi.org/10.56830/IJSIE06202302

Abdelrahman M. Farrag [*], Ahmed H. Ali [*], Waleed Abdallah [*]

[*] ***Department of Civil Engineering, Faculty of Engineering, Helwan University, Cairo 11382, Egypt.***

Abstract

The behavior and shear strength of concrete beams reinforced with longitudinal GFRP bars mixed with seawater are the subject matter of experimental research discussed in this paper. Seven beams were tested in bending to determine how much concrete contributes to shear resistance. The beams were longitudinally reinforced with glass fiber-reinforced polymer bars and were similar in size and concrete strength; however, they were not even shear-reinforced. The 3,100 mm long, 400 mm deep, and 200 mm wide beams underwent thorough testing until the failure. The test parameters included chopped fiber content (0, 0.5, 2, and 3 kg/m3), longitudinal reinforcement ratios (1.0, 1.4, and 2.0%), and mixing water type (freshwater and seawater). The test findings showed that Increasing the reinforcement ratio raised the neutral-axis depth, enabled the formation of more closely spaced cracks, and minimized the loss of flexural stiffness after cracking, according to the test results. The contribution of aggregate interlock as well as the contribution of uncracked concrete are both enhanced through increasing the area of concrete in compression. Additionally, increasing the reinforcement ratio enhances the dowel action, which reduces the tensile stresses produced in the surrounding concrete.

Keywords: Seawater; Chopped Fiber; Fiber-Reinforced Polymer (FRP); Shear Strength.

1. Introduction

The necessity of using alternative "greener" materials to create more effective and sustainable reinforced concrete (RC) structures is imposed by growing global concerns about the accumulation of construction and demolition waste and the deterioration of RC structures due to steel corrosion. Shear reinforcement is typically added to beams to prevent shear failures. Shear reinforcement is typically expensive because to the labor costs involved in installing it. In a number of applications, such as naval construction, parking structures, and bridges, noncorrosive fiber-reinforced polymer (FRP) reinforcing bars are replacing steel reinforcing bars more commonly.

(Ali, Mohamed, & Benmokrane, 2016). Additionally, in the field of tunnel excavation, the usage of glass-FRP (GFRP) bars and spirals in soft-eyes is growing in popularity in North America. Numerous studies looking into the contribution of concrete to the overall shear capacity of FRP concrete structures have been conducted recently. The experimental work has focused mainly on beams with rectangular cross sections mixed with fresh (Ali, Mohamed, & Benmokrane, 2016); (Tureyen & Frosch, 2002); (El-Sayed, 2007); (Razaqpur & Isgor, 2006). Accordingly, many models have been put forward to calculate shear capacity, most often based on a statistical curve fit to experimental beam test results (Hoult, Sherwood, Bentz, & Collins, 2008). In addition, several guidelines and standards have been published, including empirical formulae for assessing the concrete shear contribution (Nanni, 2005); (CSA-S806., 2012); (CSA-S807., 2010); (JSCE., 1997).

The aggregate interlock, uncracked concrete, residual tensile stress, and dowel-action mechanisms all contribute to the section's shear resistance in general, which is represented by the concrete shear contribution. The degree to which these mechanisms contribute is determined by the crack width, which is a result of the tension reinforcement's strain and the crack spacing (Gouda, Ali, Mohamed, & Benmokrane, 2022); (MacGregor & Wight, 2005) . Some of the shear force in the member is absorbed by the longitudinal reinforcing bars. The reinforcing bars will behave like dowels as a result of this transverse loading, which also subjects them to bending and shearing. Dowel action greatly enhances shear resistance, and the vertical displacements of the bottom reinforcement bars along the diagonal fracture surface that result in members with transverse reinforcement are constrained. Since the maximum shear in a dowel is limited by the tensile strength of the concrete cover supporting it, dowel action is often less significant when there is no shear reinforcement. when employing a significant amount of longitudinal reinforcement, especially when it is applied over several layers (Torsion, 1998), dowel action may be a significant factor. The quantity of dowel forces that can be employed in a certain circumstance is quite difficult to calculate. Several experimental studies on the operation of dowels revealed that the dowel shear force ranges from 15% to 25% of the total shear force (Torsion, 1998). Without web reinforcing, the longitudinal reinforcement ratio determines the shear strength of concrete elements.

This is explained by the fact that members with low reinforcement ratios experience broader and deeper cracks than those with high reinforcement ratios. By lowering the residual tensile stress and aggregation interlock in the fractured surface, wider cracks lessen the interface shear. Deeper fractures, on the other hand, diminish the depth of the compression zone of uncracked concrete, which lowers the contribution of uncracked concrete to the shear strength. Additionally, due to the wider use of

seawater in structural concrete, it is hypothesized to have direct environmental advantages. (Arosio, Arrigoni, & Dotelli, 2019) reported that concrete's water footprint could be reduced by up to 12% by mixing it with seawater. According to studies, the longer service life of FRP in concrete structures also clearly benefits the environment (Zhang, Lin, Abududdin, & Canning, 2011); (Cadenazzi, Dotelli, Rossini, Nolan, & Nanni, 2019); (Chen, Qu, & Zhu, 2016). For instance, (Cadenazzi, Dotelli, Rossini, Nolan, & Nanni, 2019)reported that using GFRP rather than black steel to reinforce concrete bridges results in decreases in cradle-to-grave global warming (by 25%), photochemical oxidant production (by 15%), acidification (by 5%), and eutrophication (by 50%). Together, these materials might provide significant economic advantages in addition to environmental advantages. According to a life-cycle cost estimate of seawater-mixed GFRP-reinforced concrete for high-rise buildings with a 100-year service life, the proposed concrete would be around 50% less expensive in the long run than conventional (i.e., concrete with freshwater and steel) (Younis, Ebead, & Judd, 2018).

Studies on seawater concrete have often shown a little reduction in the strength of the concrete over time (up to 10%), which is probably caused by the presence of specific ions in seawater (although these reductions depend on the curing regime used) (Nishida, Otsuki, Ohara, Garba-Say, & Nagata, 2015); (Xiao, Qiang, Nanni, & Zhang, 2017); (Dhondy, Remennikov, & Shiekh, 2019). However, these losses can be lessened by altering the mixture design, which includes using particular chemical admixtures in concrete (Li, Chen, Chu, Ouyang, & Kwan, 2019); (Younis, Ebead, Suraneni, & Nanni, 2018). The long-term strength performance of GFRP bars in seawater concrete has also been confirmed by durability studies (El-Hassan, El-Maaddawy, Al-Sallamin, & Al-Saidy, 2018); (El-Hassan, El-Maaddawy, Al-Sallamin, & Al-Saidy, Performance evaluation and microstructural characterization of GFRP bars in seawater-contaminated concrete, 2017); (Khatibmasjedi, 2018). There are few studies on the shear behavior of RC beams with seawater and chopped fiber-mixed concrete.

Given its high strength-to-weight ratio, great durability performance, and significantly lower cost compared to carbon FRPs, GFRP has demonstrated high potential as a substitute for non-corrosive reinforcement (D'Antino & Pisani, 2019). Design standards have also been created for the use of GFRP bars in RC elements, and they have been successfully implemented in a variety of structures, including bridges, parking garages, tunnels, and marine assemblies CSA-S806., 2012); (ACI440.1R-15., 2015); (Ramesh, Eswari, & Sundararajan, 2021). crack formation, the contribution from dowel action declines as the reinforcement ratio is reduced.

Research on the shear behavior of concrete members reinforced with FRP bars is

required in light of the discussion above. The experimental investigation described here is a component of a larger, on-going program of research at Helwan University that tests seven RC beam reinforcement materials that were fabricated and tested under four-point loading to evaluate various variables and design variables.

2. Experimental Program

The present study is undertaken to experimentally investigate the contribution of concrete to the shear resistance of slender beams (a/d > 2.5) longitudinally reinforced by glass fiber reinforced polymer (GFRP) bars but without shear reinforcement. The reinforcement ratio, the amount of chopped fiber, and the type of mixing water were the test variables. The actual reinforcement ratio for the FRP-reinforced concrete beams is greater than the balanced reinforcement ratio, which is described in Section 8.2.1 of ACI 440.1R-03 as:

$$\rho_{fb} = 0.85\beta_1 \frac{f_c'}{f_{fu}} \frac{E_f \varepsilon_{cu}}{E_f \varepsilon_{cu} + f_{fu}} \quad (1)$$

Figure 1. Flowchart of the methodology

2.1. Test Specimens

The goal of the experimental work for this study was to get data on the shear behavior and strength of concrete beams reinforced with FRP bars that had been mixed with seawater but without web reinforcement. A total of seven RC beams, including five reinforced with 5 glass-FRP bars (ρ = 1.0%), one with 7 glass-FRP bars (ρ = 1.4%), and one with 10 glass-FRP bars (ρ = 2.0%), were tested under two-point loading to determine the concrete contribution to their shear resistance. Figure 2 shows the dimensions, various configurations, and reinforcement details of the test specimens.

International Journal of Sustainability and Innovation in Engineering
(IJSIE)
https://www.doi.org/10.56830/IJSIE062023

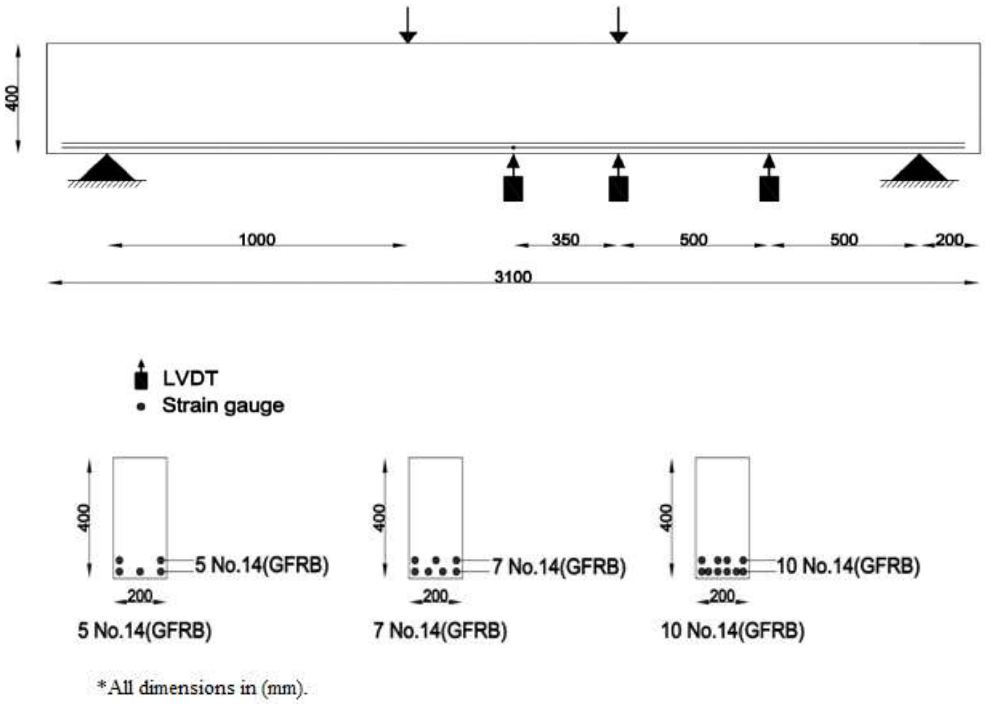

Figure 2. Test setup and cross-sectional details

Each beam was simply supported over a 2,700 mm span and had a total length of 3,100 mm, an equivalent effective flexural depth (d) of 375 mm, an equivalent effective shear depth ($d_v = 0.9d$) of 338 mm, depth of 400 mm, and width of 200 mm. The equivalent effective depths were estimated based on the shear provisions (Clause 5.8.2.9) in the 2012 edition of the *AASHTO LRFD Bridge Design Specifications*. The test parameters in this study included the effects of the reinforcement ratio, chopped fiber content, and mixing water type. The test matrix and reinforcing details for the beam specimens are shown in Table 1. The beams were designed to have a shear failure prior to flexure failure. The GFRP bars of diameter #14.0 mm were used as longitudinal reinforcement for all the tested beams.

Table 1. Details of the tested beams

Beam	Bottom Reinforcement (%)		Mixing water	hopped Fiber Conte
	Straight	ρ_f %	(Freshwater/Seawater)	(kg/m^3)
AI	5Ø14	1	Freshwater	0
BI	7Ø14	1.4	Freshwater	0
CI	10Ø14	2	Freshwater	0
AII	5Ø14	1	Freshwater	0.5
AIII	5Ø14	1	Freshwater	2
AIV	5Ø14	1	Freshwater	3
AV	5Ø14	1	Seawater	0

International Journal of Sustainability and Innovation in Engineering
(IJSIE)
https://www.doi.org/10.56830/IJSIE062023

2.2. Material Properties

The E-glass fibers utilized in the pultrusion procedure to produce the GFRP bars used in this research were impregnated with a modified vinyl-ester resin. High-modulus (HM) GFRP bars (CSA S807-10 Grade III) of 14 mm designated diameter were used in this study, as shown in Figure 3. The fiber contents in percentage by weight were 80 for the GFRP. The tensile strength and elastic modulus were calculated using the nominal cross-sectional area. The concrete used to cast each beam specimen was normal-weight concrete. The following mixture proportions were used per cubic meter of concrete: 1051 kg of coarse aggregate with a size range of 10 to 20 mm, 672 kilograms of fine aggregate, 430 kg of cement, a water-cement ratio (w/c) of 0.39, 301 mL of air entrainer, and 860 mL of water-reducing agent. Before casting, the slump was 80 mm. After 28 days, the concrete had reached the desired 35 MPa compressive strength. The actual compressive strength was calculated using the average test results of five concrete cylinders (each measuring 100 × 200 mm) tested on the same day as the start of the beam specimen testing.

Figure 3. GFRP bars

2.3. Details of Beam Fabrication

For the tested beams, seven GFRP cages were assembled. The 40 mm clear concrete cover remained unchanged. In wood formwork, the beams were prepared for casting. As shown in Figure 4, the formwork was positioned horizontally, and concrete was cast from the top. Vibration from both inside and outside was utilized. The fabrication procedure before and after casting is shown in Figure 4.

Figure 4. Fabrication process before and after casting

2.4. Instrumentation and Test Setup

With gauge lengths of 10 mm, electrical-resistance strain gauges were used to measure the strains in the longitudinal bars. Additionally, strain gauges were positioned on every shear span to gauge the diagonal strains in the concrete at the mid-shear span. Beam deflection was measured with three LVDTs placed at the mid-span and mid-shear span. The crack width was monitored by visual inspection during the test until the first crack appeared, which was initially measured with a handheld microscope. Then, seven high-accuracy LVDTs (±0.001 mm) were installed at the crack location (three at each shear span and one at the mid-span). The test setup was designed and fabricated in Helwan University's structural laboratory. A servo-controlled, hydraulic 500 kN MTS actuator connected to a spreader beam was used to load the beams in four-point bending, as shown in Figure 5. A displacement-controlled rate of 1.0 mm/min was used to apply the load. The readings of the LVDTs, load cells, and strain gauges were captured by an automatic data acquisition system controlled by a computer.

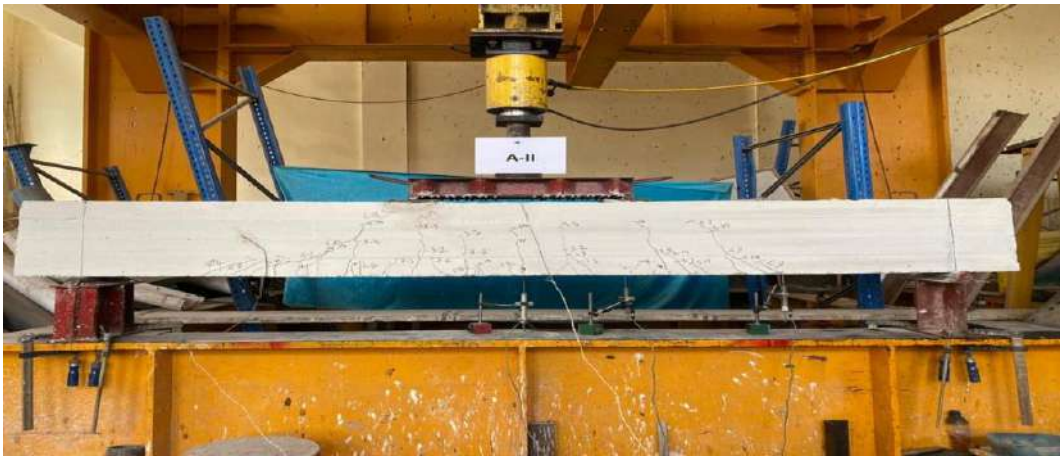

Figure 5. Experimental test setup

International Journal of Sustainability and Innovation in Engineering
(IJSIE)
https://www.doi.org/10.56830/IJSIE062023

3. Observations, Results, and Discussion

In the discussion, the measured concrete contribution to shear strength is represented by the notation (V_{exp}), and is equal to the maximum load P from the experiments. The load at which there is either a complete and abrupt failure or a sudden reduction in load carrying capability is referred to as the shear strength definition. Before the beam completely fails, a diagonal crack forms in one of the shear spans, which causes a sudden drop in load carrying capacity. Table 2 includes the test beams shear strength, (V_{exp}), as well as other relevant data. The experimental test findings in terms of deflection values and ultimate shear load (V_{exp}), and the measured strain in the longitudinal reinforcement (ε_u), modes of failure, and deflection, will be detailed in the following discussion includes the effect of the test variables on the ultimate shear strength and behavior of the tested beams.

Table 2. Experimental shear strength and deflection values for tested beams

Beam	Reinforcement		Mixing water (Freshwater/Seawater)	$V_{EXP.}$ (ton)	Deflection (mm)		
	(ρ_f) %	No. of bars			At mid-span	Under point load	Between Point load and support
A-I	1	5	Freshwater	10.0659	17.653	15.745	8.304
B-I	1.4	7	Freshwater	11.148	12.423	11.643	6.784
C-I	2	10	Freshwater	13.87	7.534	6.347	5.326
AII	1	5	Freshwater	10.176	17.425	15.554	8.154
AIII	1	5	Freshwater	11.2	16.257	15.382	7.897
AIV	1	5	Freshwater	10.3	15.78	14.975	7.468
AV	1	5	Seawater	10.1994	16.754	15.724	8.075

3.1. Effect of Test Parameters on Load–Deflection Behavior

To illustrate the effects of various parameters on the shear behavior of RC-GFRP beams, as shown in Figure 6, this section presents the load-deflection curves for the tested beams in three groups. Before cracking, the tested beams exhibited linear load-deflection behavior. Using the gross moment of inertia of the concrete cross section, the stiffness of the beam at this stage was essentially comparable independent of the amount and type of reinforcement. As the load increased after cracking, stiffness decreased. At this stage, the longitudinal reinforcement's area and elastic modulus, which determine the axial stiffness of the reinforcing bars, were a factor in flexural stiffness, which was a function of those parameters (Ali, Mohamed, & Benmokrane, 2016).

International Journal of Sustainability and Innovation in Engineering
(IJSIE)
https://www.doi.org/10.56830/IJSIE062023

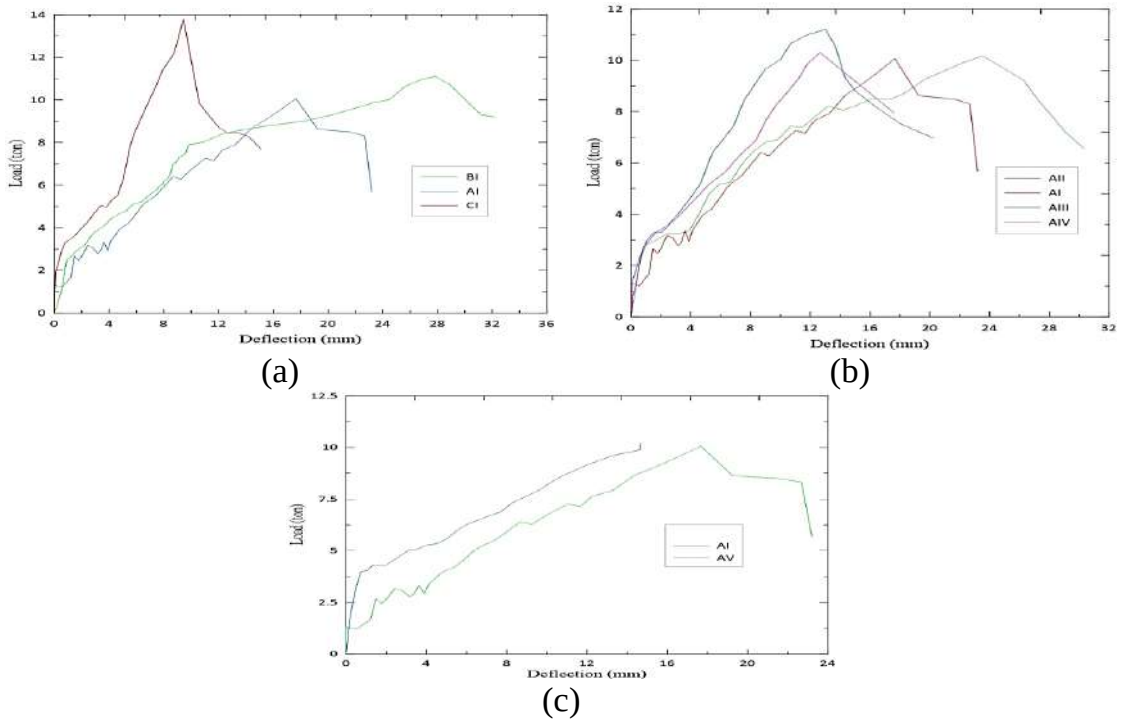

Figure 6. Effect of test parameters on load-deflection behavior

Figure 6-a shows the effect of reinforcement type on the load-deflection behavior. The three GFRP reinforced beams (A-I, B-I, and C-I) were designed to have a flexural-reinforcement ratio as 1%, 1.4%, and 2.0%, respectively. Nevertheless, the increase in deflection immediately after cracking was more significant in the GFRP-reinforced beams with a lower reinforcement ratio of 1%. This illustrates the effect of the reinforcing bars' elasticity modulus on the stiffness of the flexural after-cracking. The figure demonstrates that the post-cracking flexural stiffness for the beam strengthened with 5 GFRP bars (1%) was lower than that of the beam reinforced with 10 GFRP bars (2.0%). The average ratio between the post-cracking flexural stiffness of the GFRP-reinforced beam with a 2.0% reinforcement ratio to the GFRP-reinforced beam with 1% reinforcement ratio was approximately 1.45. These ratios were approximately the same as the ratios of the modulus of elasticity of steel to that of FRP bars. Therefore, it can be concluded that the post-cracking flexural stiffness was equal to the ratio of the axial stiffness of the FRP reinforcing bars. This is in good agreement with the results of (Ali, Mohamed, & Benmokrane, 2016); (Tureyen & Frosch, 2002); (El-Sayed, 2007). Figure 6-a, indicate that, after cracking, the flexural stiffness of the GFRP-RC beams CI (k_u= 31.5 kN/m) and BI (k_u= 23.6 kN/m) was almost 3 and 2.3 times of that of the GFRP-RC beam AI (k_u= 10.2 kN/m). Thus, the flexural behavior of the tested beams seems to have been a function of the axial stiffness of the reinforcing bars. Since the deflection behavior of a beam reflects its stiffness inversely proportions to it, according to the slope of the initial deflection at the linear stage of

loading, the beam (C1) had an initial stiffness more than the (AI and BI) by 45%.

The effect of chopped fibers on the behavior and strength of FRP-reinforced concrete beams is shown in Figure 6-b. As shown in Figure 6-b, which illustrates that when adding chopped fibers by 2 and 3 kg/m^3, the ultimate load and stiffness of the beam increased while the deflection decreased at the same load level. These results show the good response of specimens having chopped fibers, especially the 3 kg/m^3 ones, compared with those that have not. The physical interpretation of these results is that increasing the chopped fiber has more ability to prevent potential cracks in the tension zone from initiating than beams without chopped fibers.

Figure 6-c shows the effect of seawater on the behaviour and strength of beams reinforced with FRP bars. The figure showed that the effect of seawater immersion has an impact on the decrease in the maximum load capacity of the beam. The decrease in load capacity occurs along with the immersion time.

3.2. Crack Pattern and Modes of Failure

Diagonal tension failure resulted from the diagonal shear crack extending toward the loading point. The beams were loaded gradually till failure load occurs as shown in Figure 7.

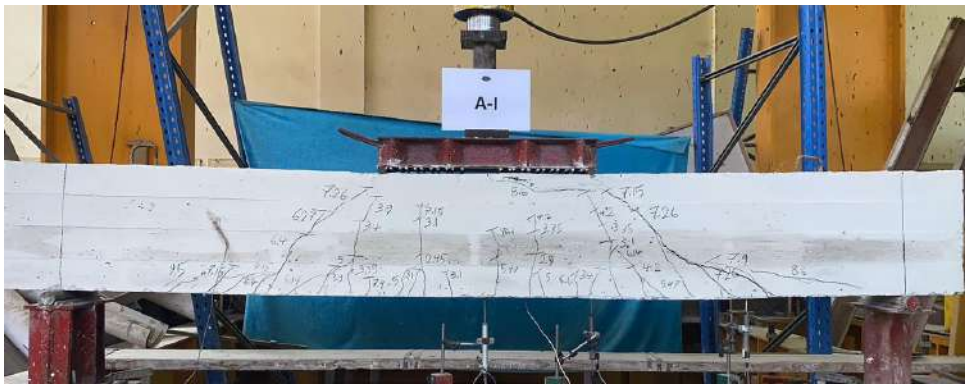

(a)

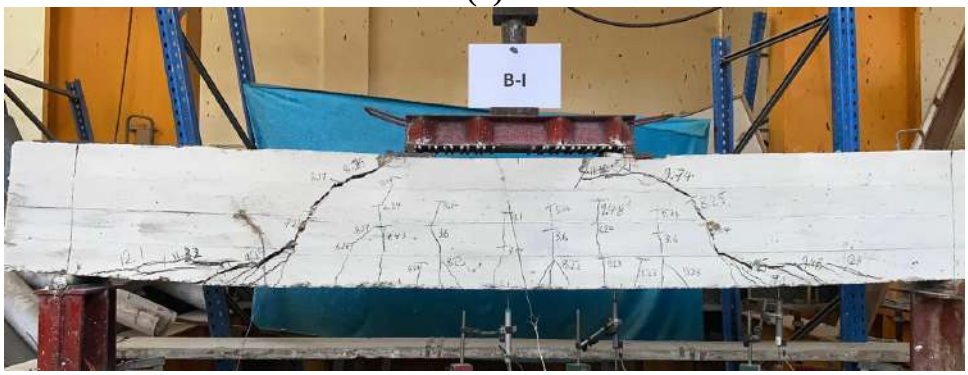

(b)

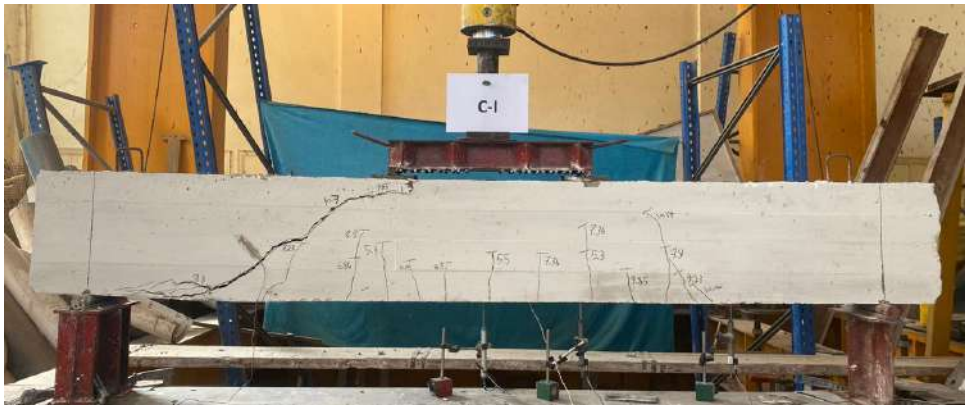

(c)

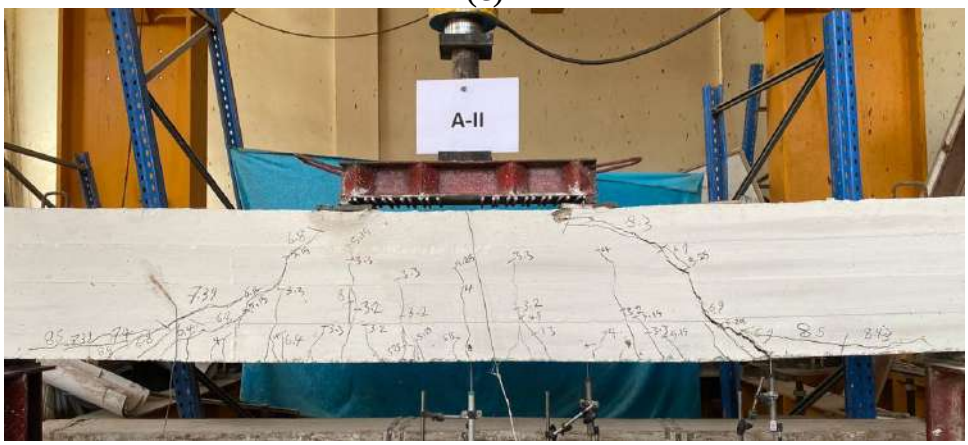

(d)

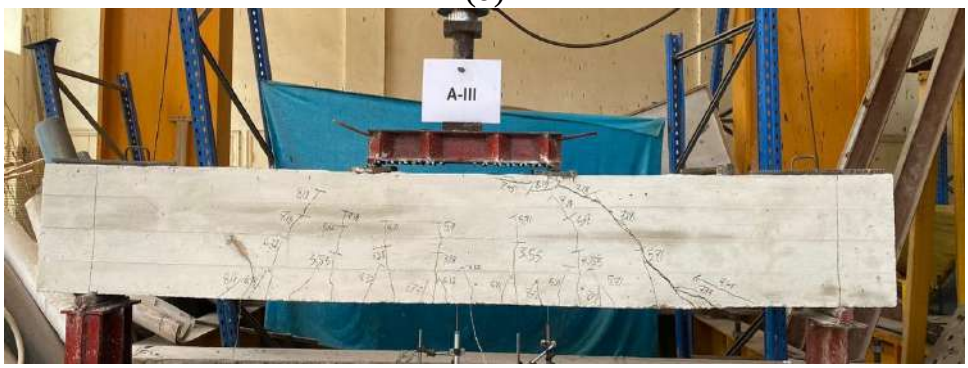

(e)

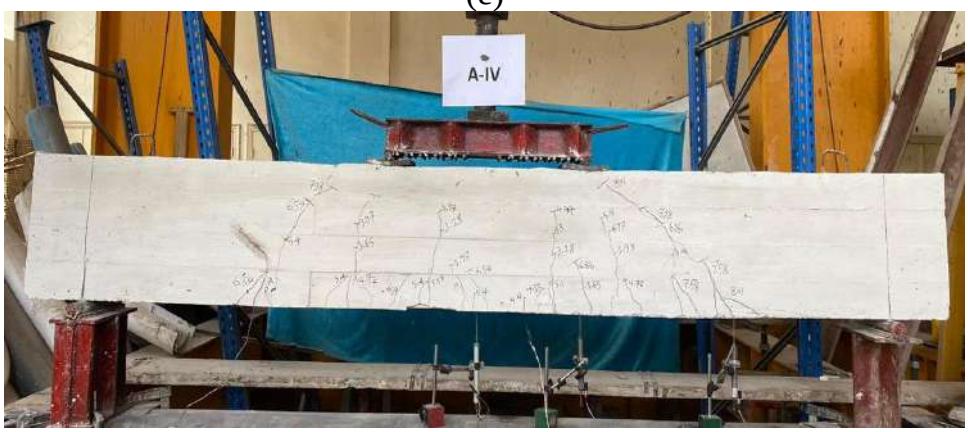

(f)

International Journal of Sustainability and Innovation in Engineering
(IJSIE)
https://www.doi.org/10.56830/IJSIE062023

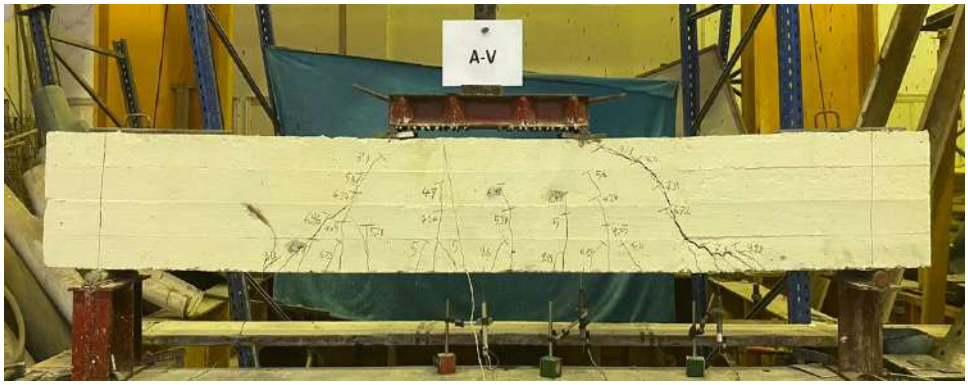

(g)

Figure 7. Crack pattern and modes of failure

It's observed that the failure modes for the beams were almost similar, it happened at the shear zone. Upon increasing the load, more flexure cracks appeared in the bottom of the tension zone and expanded vertically upward. After that at different loading stages, the flexural-shear cracks propagated and increased in number at a higher rate than their vertical expanding. Then the shear cracks began to propagate at a higher rate. Also shear cracks occurred at the top of the beam below the loading points at high loading stages. The shear cracks expanded gradually until they caused the shear failure for the concrete.

The first crack in beams (AI, BI, CI) was discovered at mid-span bottom fiber by 2.4-, 3.2- and 4.3-ton load respectively as shown in Figure 8-a. Regardless of the type of reinforcement, it was generally found that specimens with lower reinforcement ratios (AI) failed in brittle shear with few visible diagonal shear cracks. The specimens (BI and CI) with larger reinforcement ratios showed less brittle shear failure and the formation of many diagonal cracks. The final cracking pattern for each test specimen is shown in Figure 7. The thick lines show cracks that developed at failure, while the lighter ones show cracks that developed earlier. In a specimen with a high reinforcement ratio, severe cover spalling was seen at the ultimate load on the upper surface of the beam (CI). This is explained by the fact that, when shear failure was about to occur, more inclined upper cracks spread from the diagonal-tension shear crack back towards the support. The opening of the inclined failure crack effectively causes the aggregate interlock to be lost, hence the net shear transfer was dispersed across the section. To maintain cross-sectional equilibrium, the longitudinal reinforcement's dowel action, which was distributed evenly throughout the section, had to be increased. The concrete around the bars experienced a vertical tensile stress as a result of the sudden increase in dowel action in these bars. This was significant enough to cause cover spalling and splitting along the plane of the reinforcement when combined with the existing splitting stresses put on by the flexural bond.

International Journal of Sustainability and Innovation in Engineering
(IJSIE)
https://www.doi.org/10.56830/IJSIE062023

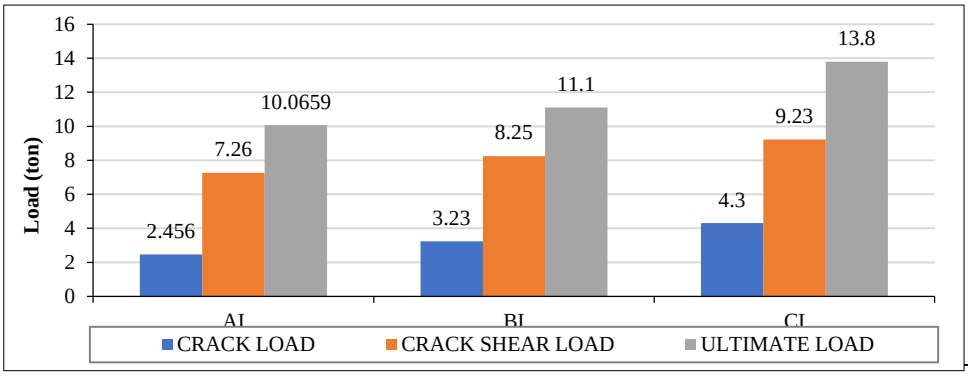

(a)

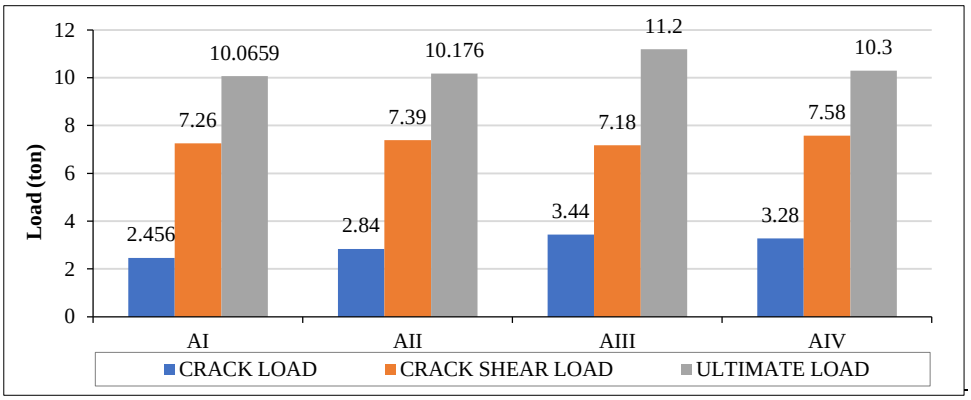

(b)

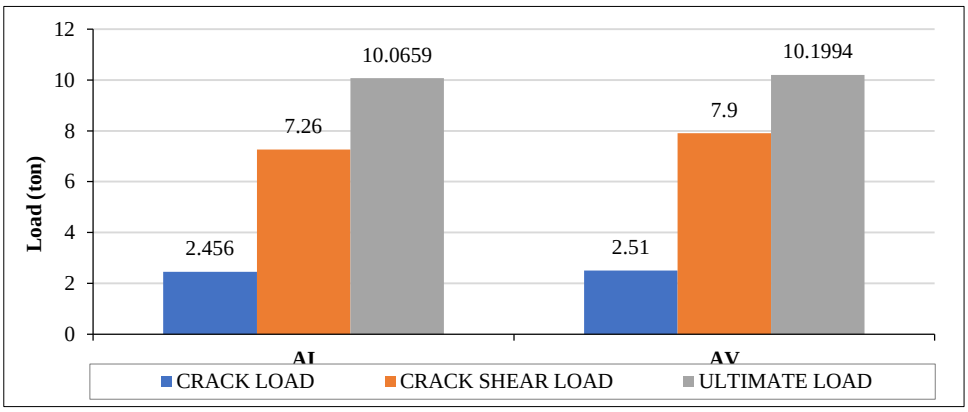

(c)

Figure 8. Comparison of the cracking, shear crack and ultimate loads for beams

International Journal of Sustainability and Innovation in Engineering
(IJSIE)
https://www.doi.org/10.56830/IJSIE062023

For beams (AI, AII, AIII and AIV and AV), the first crack was observed in the mid-span at 2.4, 2.8, 3.44 and 3.28 and 2.51 ton load respectively as observed in Figure 8-b. It's shown that, At the chopped fiber content of 0.5, 2 and 3 kg/m^3, the cracking load was greater than the cracking load of the specimen AI with 0 kg/m^3 by 4%, 10% and 8% respectively. However, when the chopped fiber content increases from 2 to 3 kg/m^3 the cracking load decreases by 9%, and this would be explained by that the chopped fiber content with a high ratio may not be mixed well with the concrete specially with chopped glass fiber which may causes a void and be a week zone in tension in the concrete. So, it must be sure that the chopped fiber is well distributed in the concrete to reach the required homogeneity.

At the mid-span for beams (AI and AV), the first crack was obtained at 2.4- and 2.51-ton load respectively as shown in Figure 8-c. We can find that using in concrete mixtures has little to no effect in the short-term on the cracking load instead of using freshwater. using seawater increases the cracking load than using freshwater by 2% and 3% respectively.

3.3. Shear Capacity of Concrete Beams

The definition of shear failure used herein describes the formation of inclined shear (diagonal-tension) cracking and the subsequent sudden drop in load-carrying capacity. Shear capacity is defined as the load at which complete or abrupt failure occurs (Yost, Goodspeed, & Schmeckpeper, 2001). Beams (AI, BI and CI) failed in diagonal tension. Figure 8-a, and Figure 9 give the effect of the reinforcement ratio on the shear strength of the tested beams.

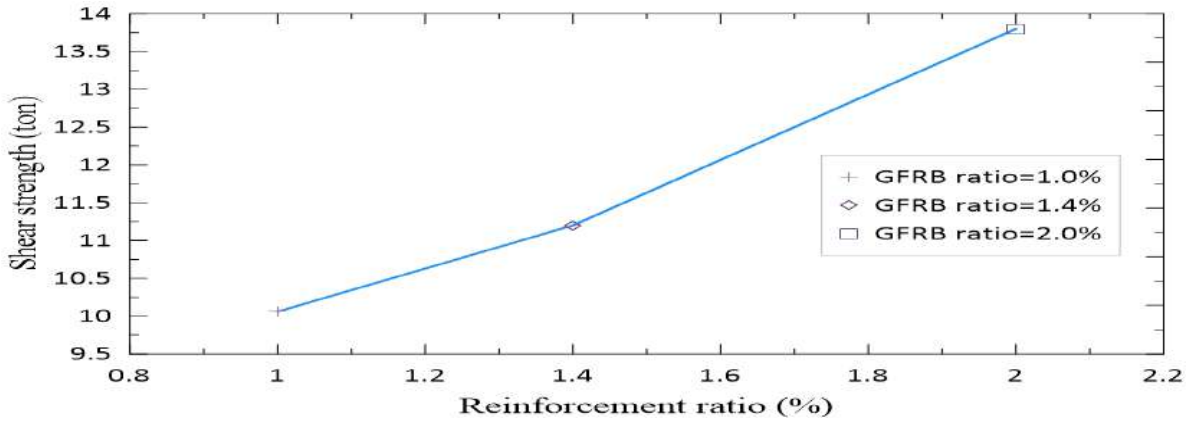

Figure 9. Shear strength versus reinforcement ratio

The figures show that as the reinforcement ratio increased, the shear strength of the GFRP-reinforced beams increased. Shear strengths increased by 11.0% and 37%, respectively, when the reinforcement ratio was increased by about 40% and 100%

International Journal of Sustainability and Innovation in Engineering
(IJSIE)
https://www.doi.org/10.56830/IJSIE062023

(from 1.0% to 1.4% and from 1.0% to 2.0%). The shear strengths were also increased by 24% by increasing the reinforcement ratio by 40% (from 1.4% to 2.0%). For the beam with the highest reinforcement ratio, the increase in shear strength was more pronounced. By increasing the neutral-axis depth and enabling the formation of more closely spaced cracks, the use of additional reinforcement dispersed across the cross section reduces the loss of flexural stiffness after cracking. By increasing the area of concrete in compression, this in turn enhances the contribution of aggregate interlock as well as the contribution of uncracked concrete. Furthermore, raising the reinforcement ratio improves the dowel action, which reduces the tensile stresses which are created in the surrounding concrete.

Beams (AI, AII, AIII and AIV) failed in diagonal tension. Figure 8-b gives the effect of the chopped fiber on the shear strength of the tested beams. The figure indicates that the shear strength in the GFRP-reinforced beams increased as the chopped fiber increased till the content of 2 kg/m^3, after that the shear strength decreases when the chopped fiber content increases to 3 kg/m^3. Increasing the chopped fiber content (from 0 to 0.5 kg/m^3, from 0 to 2.0 kg/m^3 and from 0 to 3.0 kg/m^3) increased the shear strengths by 1.0%, 11% and 2%, respectively. However, increasing the chopped fiber content (from 2 to 3 kg/m^3) decreased the shear strengths by 8%.

Beams (AI and AV) failed in diagonal tension. Figure 8-c gives the effect of the mixing water type on the shear strength of the tested beams. The figure indicates that the shear strength in the GFRP-reinforced beams had a slightly increasing with seawater mixing. Seawater mixing increased the short term of shear strengths by 1.0%.

3.4. Strains in the FRP Longitudinal Reinforcement

For the internal GFRP longitudinal bars, Figure 10 shows the measured applied load on the beams versus the strain relationships.

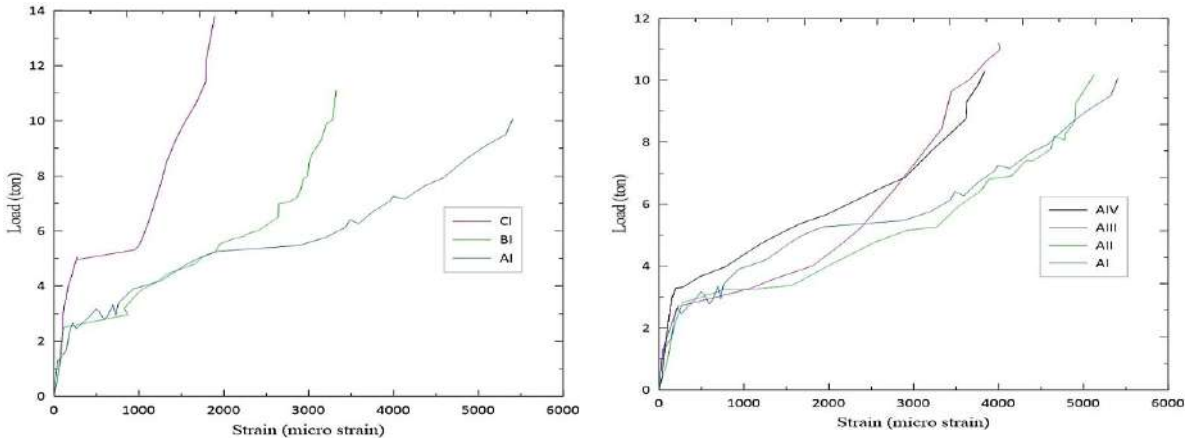

(a) (b)

International Journal of Sustainability and Innovation in Engineering
(IJSIE)
https://www.doi.org/10.56830/IJSIE062023

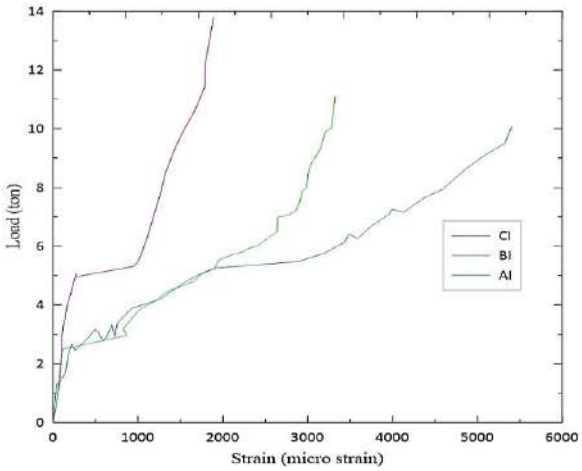

(c)

Figure 10. GFRP bar stress-strain relationship

For beams (AI, BI and CI) the longitudinal reinforcing bars of the FRP specimens had very little strain up until the concrete section cracked, as illustrated in Figure 10-a. Up until this phase, the GFRP specimens showed strain behaviors that were comparable. At the same load level, after cracking the concrete beam reinforced with a greater reinforcement ratio (CI) showed less bar strain than the beams reinforced with FRP (AI and BI), as the latter had relatively lower elastic moduli than the specimen CI. Throughout the testing, no specimen's FRP longitudinal reinforcement strain reached 50% of the ultimate tensile strain of the bars. None of the beams showed any indications of anchorage issues. The maximum strains in FRP bars were approximately 5450, 3300, and 1900, microstrains for AI, BI, and CI, respectively. In general, this relatively low strain at ultimate in the beams reinforced with FRP bars shows that shear failure was not triggered by the FRP bars rupturing.

For beams (AI, AII, AIII and AIV), up until the concrete section cracked, there was little strain in the longitudinal reinforcing bars of the FRP specimens. The concrete beams mixed with higher chopped fiber content (AIII and AIV) exhibited less bar strain than the beams mixed with lower chopped fiber content (AI and AII) at the same load level as shown in Figure 10-b. The maximum strains in FRP bars were approximately 5400, 5150, 4000 and 3850, microstrains for AI, AII, AIII and AIV, respectively.

For beams (AI and AV) up until the concrete section cracked, there was little strain in the longitudinal reinforcing bars of the FRP specimens as shown in Figure 10-c. The concrete beams mixed with seawater (AV) exhibited less bar strain than the beams mixed with freshwater (AI) at the same load level. The maximum strains in FRP bars were approximately 5450 and 4000, microstrains for AI, and AV, respectively.

3.5. Shear Crack Width

During the experimental test, it was found that increasing the reinforcement ratio minimized the shear-crack width. Therefore, at the same stress level, shear-crack width decreases as reinforcement ratio increases. Wider cracks were observed on the GFRP-reinforced beam (AI) the GFRP-reinforced one (BI and CI).

4. Conclusions

This paper presents experimental work to investigate the shear behaviour of beams reinforced with GFRP bars and mixed with seawater and chopped fiber. A total of seven full-scale RC specimens were prepared to study the effect of the reinforcement ratio, mixing water, and chopped fiber content on the shear behavior. Based on the experimental test results and analysis presented in this paper, the following conclusions can be drawn:

- Diagonal tension failure was the observed failure mode of the tested FRP reinforced beams.
- The axial stiffness of the reinforcing bars controls the load-deflection behavior of the beams after cracking.
- With an increase in the reinforcement ratio, the shear strength of beams increases.
- The axial stiffness of the longitudinal reinforcing bars affects how much concrete contributes to the shear strength of RC beams V_{cf}. The shear strength obtained increases with increasing reinforcement ratios or elastic modulus of the reinforcing bars.
- The cracking load of beams with 2% reinforcement ratio is 35% greater than 1% reinforcement ratio and beams with 1.5% reinforcement ratio is 15% greater than 1% reinforcement ratio.
- At the chopped fiber content of 0.5, 2 and 3 kg/m^3, the cracking load was greater than the cracking load of the specimens with 0 kg/m^3 by 4%, 10% and 8% respectively. However, when the chopped fiber content increases from 2 to 3 kg/m^3 the cracking load decreases by 9%.
- The results suggest that the use of seawater in concrete has insignificant effects on the shear capacity of RC beams, using seawater increases the cracking load and cracking shear load than using freshwater by 2% and 3%, respectively. On the other hand, it increases the shear strength by 5%.

4.1. Recommendations

The results shown above, specifically the numbers, are based only on the materials and samples used in this investigation. Finally, it should be noted that the current study only evaluates the short-term shear performance of reinforced concrete beams. It is crucial that future research investigate the long-term effects of chemicals in seawater on GFRP-reinforced concrete beams. Further study is required to study the torsional and fatigue behaviors of reinforced concrete beams when reinforced with the proposed combination (seawater + chopped fiber + GFRP).

5. References

ACI440.1R-15. (2015). Guide for the Design and Construction of Structural Concrete Reinforced with Fiber-Reinforced Polymer (FRP) Bars. *American Concrete Institute (ACI), Michigan, United States*.

Ali, A. H., Mohamed, H. M., & Benmokrane, B. (2016). Shear Behavior of Circular Concrete Members Reinforced with GFRP Bars and Spirals at Shear Span-to-Depth Ratios between 1.5 and 3.0. *Journal of Composites for Construction, 20(6)*.

Arosio, V., Arrigoni, A., & Dotelli, G. (2019). Reducing water footprint of building sector: Concrete with seawater and marine aggregates. *IOP Conference Series: Earth and Environmental Science, 323(1)*, 12127.

Cadenazzi, T., Dotelli, G., Rossini, M., Nolan, S., & Nanni, A. (2019). Life-cycle cost and life-cycle assessment analysis at the design stage of a fiber-reinforced polymer-reinforced concrete bridge in Florida. *Advances in Civil Engineering Materials, 8(2),20180113*.

Chen, L., Qu, W., & Zhu, P. (2016). Life cycle analysis for concrete beams designed with cross-sections of equal durability. *Structural Concrete, 17(2)*, 274–286.

CSA-S806. (2012). Design and Construction of Building Components with Fibre-Reinforced Polymers. Canadian Standards Association (CSA). *Toronto, Canada*.

CSA-S807. (2010). Specification for Fibre-Reinforced Polymers. Canadian Standards Association (CSA). *Toronto, Canada*.

D'Antino, T., & Pisani, M. A. (2019). Long-term behavior of GFRP reinforcing bars. *Composite Structures, 227, 111283.*

Dhondy, T., Remennikov, A., & Shiekh, M. N. (2019). Benefits of using sea sand and seawater in concrete: a comprehensive review. *Australian Journal of Structural Engineering, 20(4)*, 280–289.

El-Hassan, H., El-Maaddawy, T., Al-Sallamin, A., & Al-Saidy, A. (2017). Performance evaluation and microstructural characterization of GFRP bars in seawater-contaminated concrete. *Construction and Building Materials, 147*, 66–78.

El-Hassan, H., El-Maaddawy, T., Al-Sallamin, A., & Al-Saidy, A. (2018). Durability of glass fiber-reinforced polymer bars conditioned in moist seawater-contaminated concrete under sustained load. *Construction and Building Materials, 175*, 1–13.

El-Sayed, A. A. (2007). Concrete contribution to the shear resistance of FRP-reinforced concrete beams. *PhD Thesis, Université de Sherbrook, Sherbrook, Canada*.

Gouda, A., Ali, A. H., Mohamed, H. M., & Benmokrane, B. (2022). Analysis of circular concrete members reinforced with composite glass-FRP spirals. *Composite Structures, 297*, 115921.

Hoult, N. A., Sherwood, E. G., Bentz, E. C., & Collins, M. P. (2008). Does the Use of FRP Reinforcement Change the One-Way Shear Behavior of Reinforced Concrete Slabs? . *Journal of Composites for Construction, 12(2)*, 125–133.

JSCE. (1997). Recommendation for design and construction of concrete structures using continuous fiber reinforcing materials. *Japan Society of Civil Engineers, Tokyo, Japan*.

Khatibmasjedi, M. (2018). Sustainable concrete using seawater and glass fiber reinforced polymer bars. *PhD Thesis, University of Miami, Coral Gables, United States*.

Li, L. G., Chen, X. Q., Chu, S. H., Ouyang, Y., & Kwan, A. K. (2019). Seawater cement paste: Effects of seawater and roles of water film thickness and superplasticizer dosage. *Construction and Building Materials, 229, 116862*.

MacGregor, J. K., & Wight, J. G. (2005). Reinforced Concrete: Mechanics and Design (4th Ed.). *Prentice-Hall, Upper Saddle River, United States*.

Nanni, A. (2005). Guide for the Design and Construction of Concrete Reinforced with FRP Bars (ACI 440.1R-03). *Structures Congress*.

Nishida, T., Otsuki, N., Ohara, H., Garba-Say, Z. M., & Nagata, T. (2015). Some Considerations for Applicability of Seawater as Mixing Water in Concrete. *Journal of Materials in Civil Engineering, 27(7)*.

Ramesh, B., Eswari, S., & Sundararajan, T. (2021). Experimental and numerical studies on the flexural behaviour of GFRP laminated hybrid-fibre-reinforced concrete (HFRC) beams. *Innovative Infrastructure Solutions, 6*, 1-13.

Razaqpur, A. G., & Isgor, O. B. (2006). Proposed shear design method for FRP-reinforced concrete members without stirrups. *ACI Structural Journal, 103(1)*, 93.

Torsion, A.-A. C. (1998). Recent approaches to shear design of structural concrete. *Journal of structural engineering, 124(12)*, 1375-1417.

Tureyen, A. K., & Frosch, R. J. (2002). Shear tests of FRP-reinforced concrete beams without stirrups. *Structural Journal, 99(4)*, 427-434.

Xiao, J., Qiang, C., Nanni, A., & Zhang, K. (2017). Use of sea-sand and seawater in concrete construction: Current status and future opportunities. *Construction and Building Materials, 155*, 1101–1111.

Yost, J. R., Goodspeed, C. H., & Schmeckpeper, E. R. (2001). Flexural Performance of Concrete Beams Reinforced with FRP Grids. *Journal of Composites for Construction, 5(1)*, 18–25.

Younis, A., Ebead, U., & Judd, S. (2018). Life cycle cost analysis of structural concrete using seawater, recycled concrete aggregate, and GFRP reinforcement. *Construction and Building Materials, 175*, 152–160.

Younis, A., Ebead, U., Suraneni, P., & Nanni, A. (2018). Fresh and hardened properties of seawater-mixed concrete. *Construction and Building Materials, 190*, 276–286.

Zhang, C., Lin, W. X., Abududdin, M., & Canning, L. (2011). Environmental Evaluation of FRP in UK Highway Bridge Deck Replacement Applications Based on a Comparative LCA Study. *Advanced Materials Research, 374–377*, 43–48.

Journal of Sustainability and Innovation in Engineering
(IJSIE)
https://www.doi.org/10.56830/IJSIE062023

Effect of Fire on Concrete Contribution to Shear Resistance of GFRP RC Beams

https://www.doi.org/10.56830/IJSIE06202303

Mahmoud Mehany

Department of Civil and Building Engineering

University of Helwan, Cairo, Egypt
eng.mahmoud.abdelghafar@gmail.com

Abstract

The use of fiber-reinforced polymer (FRP) bars is becoming commonplace in various civil engineering applications due to the several advantages they offer over traditional materials. However, limited knowledge about some aspects of the behavior of FRP bars, particularly when subjected to severe fires, is hampering their widespread use. This paper presents the results of a research program to investigate the shear behavior of glass-FRP (GFRP)-reinforced beams exposed to severe fires. Three reinforced concrete (RC) beam specimens with a cross-sectional width and height of 150 mm and 300 mm, respectively, and with a total length of 1700 mm were constructed and tested under four-point bending load up to failure. The main test variables were the reinforcement ratio and the fire. The experimental results show that all beams failed as a result of diagonal tension cracking. The shear resistance and stiffness of the RC beams decreased when the beams are exposed to fire at the same reinforcement ratio.

Keywords*: GFRP bars, reinforced concrete beams, fire, shear capacity, crack patterns, modes of failure.*

Introduction

Nowadays, fiber-reinforced polymer (FRP) bars are being more accepted in many design codes ((CSA), 2012); (Canadian, 2019); (American, 2015) as an alternative reinforcement to conventional steel bars in reinforced concrete (RC) members. Among the different types of FRP bars, Glass-FRP (GFRP) bars are widely used as longitudinal reinforcement in North America due to their superior performance. In addition to its excellent corrosion resistance, GFRP reinforcement has a high strength-to-weight ratio, good fatigue properties as well as good resistance to chemical attack and electromagnetic resistance. GFRP bars can be used in concrete structural members such as foundations, breakwaters, and other structures subjected

Journal of Sustainability and Innovation in Engineering
(IJSIE)
https://www.doi.org/10.56830/IJSIE062023

to harsh environmental effects exhibit good resistances to chemical aggressiveness and fire.

Significant effort has been given in the last decades to study the behavior of FRP RC elements and to improve the design guidelines, especially the shear design equations. Current shear design provisions of FRP RC elements are based on experimental data mostly obtained from shear testing of RC beams. The concrete contribution to the shear resistance of the section represents the shear resisted by various shear mechanisms. ACI-ASCE Committee 445 (ASCE-ACI, 1998) assessed that the quantity of concrete shear strength can be considered as a combination of five mechanisms activated after the formation of diagonal cracks: (1) uncracked concrete, (2) aggregate interlock, (3) dowel action of the longitudinal reinforcement, (4) arch action, and (5) residual tensile stresses across the inclined crack (see Fig. 1). The contribution of the uncracked concrete in RC elements depends mainly on the concrete strength and on the depth of the uncracked zone, which is function of the longitudinal reinforcement properties.

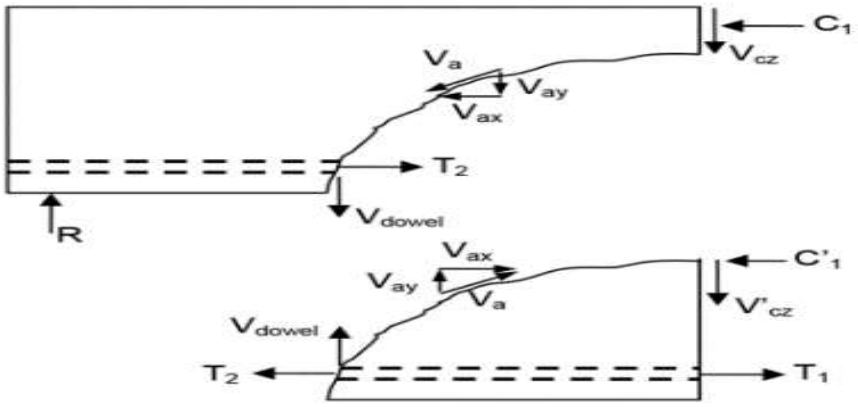

where:
R = reaction
C_1, C'_1 = compression forces
T_1, T_2 = tension forces
V_{cz} = shear transferred in the uncracked concrete (flexural compression zone)
V_a = interface shear transfer (aggregate interlock)
V_{dowel} = dowel shear

Fig (1) : Internal forces in cracked beam without stirrups (MacGregor & Wight, 2005).

Generally, there is a paucity of the experimental studies regarding RC members reinforced with FRP bars under fire exposure (Nigro, G. Cefarelli, Bilotta, & Cosenza, 2011); (Hajiloo, Green, Noël, Bénichou, & Sultan., 2017); (Gooranorimi, Claure, De Caso, Suaris, & Nanni, 2018); (Hajiloo, H.; Green, M. F.; Noël, M.; Bénichou, N.; Sultan, M., 2019). (Nigro, G. Cefarelli, Bilotta, & Cosenza, 2011);

(Hajiloo, Green, Noël, Bénichou, & Sultan., 2017) showed that the bond failure of fire exposed GFRP RC slabs can be prevented by providing sufficiently long unexposed (cool) regions to ensure adequate anchorage of the bars. (Gooranorimi, Claure, De Caso, Suaris, & Nanni, 2018) exposed six small-scale 2000 mm long GFRP RC slabs to (ASTM., 2015) standard fire. The slabs were similar to each other with the exception of the surface treatments of the reinforcing bars; three of the slabs were reinforced with sand coated GFRP bars, and the other three slabs were reinforced with bars with surface deformations. The test results indicated that the GFRP bars were not severely damaged from two hours of heat exposure with the low elevated temperature exposure. (Hajiloo, H.; Green, M. F.; Noël, M.; Bénichou, N.; Sultan, M., 2019). Investigated the fire resistance of two full-scale GFRP RC slabs with only 40 mm of clear concrete cover and 200 mm of unexposed (cool) anchor zone at the ends. Both slabs endured 3 h under the standard fire. The slabs were loaded with a sustained load, which caused a moment equal to 45% of their ultimate flexural strength. The temperature reduces significantly in the unexposed zones, providing an adequate anchorage for the bars when almost the entire GFRP-to-concrete bond deteriorated in the exposed zone. Their results enabled an efficient, economic, and fire-safe application of GFRP reinforcement in concrete construction by reducing the concrete cover.

Objectives

This investigation is a part of an extensive research program on the behavior of RC beams reinforced with GFRP under various loading conditions, which was carried out at the Helwan University. The objectives of this study were (1) to explore the feasibility and efficiency of using GFRP bars on RC beams under fire; (2) to investigate the influence of the GFRP reinforcement ratio on the concrete contribution to shear behavior of the specimens; and (3) to analyze the effect of fire on concrete shear capacity.

Expermental Program

Materials

The beams were constructed using normal-weight concrete (NWC) with a target compressive strength of 25 MPa after 28 days at room temperature. Table I gives the mixture proportions of the NWC used in this study. The actual compressive strengths of concrete, *f'c*, were determined in accordance with (C39/C39M-18., 2018) from six concrete cylinders (100 x 200 mm) for the NWC. All cylinders were cured under identical conditions with the beams

Table (1):NWC mix proportions.

Concrete	
w/c	0.38
Water (Kg/m3)	210
Cement type	Portland cement
Cement content (Kg/m3)	382
Fine aggregate content (Kg/m3)	570
Coarse aggregate content (Kg/m3)	1200
Coarse aggregate size (mm)	10 to 20
Slump (mm)	85

The glass FRP bars employed in this study were manufactured and developed in Egypt. The bars were made of continuous longitudinal fibers impregnated in a thermosetting vinyl-ester resin with a typical fiber content of 73 %. Number 4 (12.7 mm diameter) bars with nominal cross-sectional areas of 129 mm2 were used to reinforce the beam specimens in the longitudinal direction. Fig. 2 shows the stress-strain relationship of the GFRP bars as measured by standard tension tests in accordance with (ACI, 2004) (see Fig. 2). Fig. 3 illustrates the surface characteristics of the GFRP bars. In this investigation, the nominal values were selected for use in designing the beam specimens and in all analyses. The modulus of elasticity, ultimate tensile strength, and strain at rupture were estimated according to (ASTM, 2011). Table II presents the mechanical characteristics of the GFRP bars. Mild smooth steel bars of 8 mm diameter were used as top reinforcement to hold the stirrups behind the supports. Furthermore, one size of steel stirrups (8 mm diameter) was fabricated to use behind the supports for all the beams.

Table (2): Mechanical properties of the GFRP reinforcement

Bar type	GFRP bars
Bar size	No. 4
Diameter (mm)	12.7
Af a (mm^2)	129
Aim b (mm^2)	138 ± 2
Ef (GPa)	42.0 ± 1.5
ffu (MPa)	749 ± 27
εfu (%)	1.2

a Nominal cross-sectional area.
b Immersed cross-sectional area (measured).
Note: Properties calculated based on the nominal cross- sectional area.

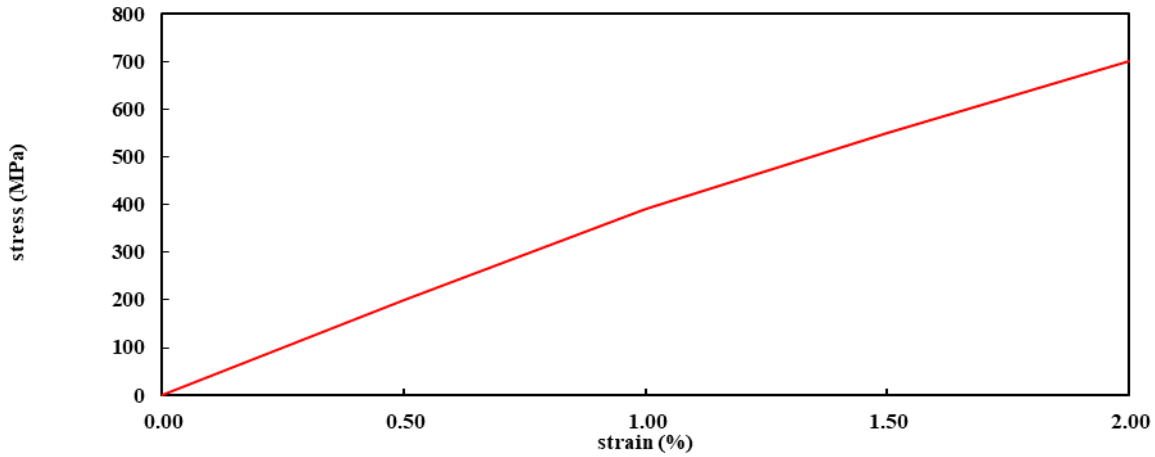

Fif (2): Tensile test of GFRP bars.

Fif (3): Surface characteristics GFRP bars.

Beam Design, Fabrication and Details

Three RC beam specimens measuring 150 × 300 mm were tested in this study, with a total span of 1700 mm. All beams were reinforced with GFRP bars. Two RC beams are exposed to fire, while the other one was used as a reference specimen. The influence of GFRP reinforcement ratio on the shear behavior was investigated by testing two beams reinforced longitudinally with No. 4 GFRP bars with reinforcement ratios of 2.3% and 1.0%. Two 8 mm steel bars were used as top reinforcement to hold the stirrups behind the supports. In addition, three stirrups 8 mm at each end were used to prevent anchorage failure. The details of the reinforcement and the tested beams are illustrated in Fig. 4. Each beam is identified with a label consisting of numbers and letters, beginning with B referring to the concrete member: Beam. The numbers 1 and 2 represent the longitudinal

Journal of Sustainability and Innovation in Engineering
(IJSIE)
https://www.doi.org/10.56830/IJSIE062023

reinforcement ratio, followed by the fire duration. Table III gives the test matrix of the beam specimens.

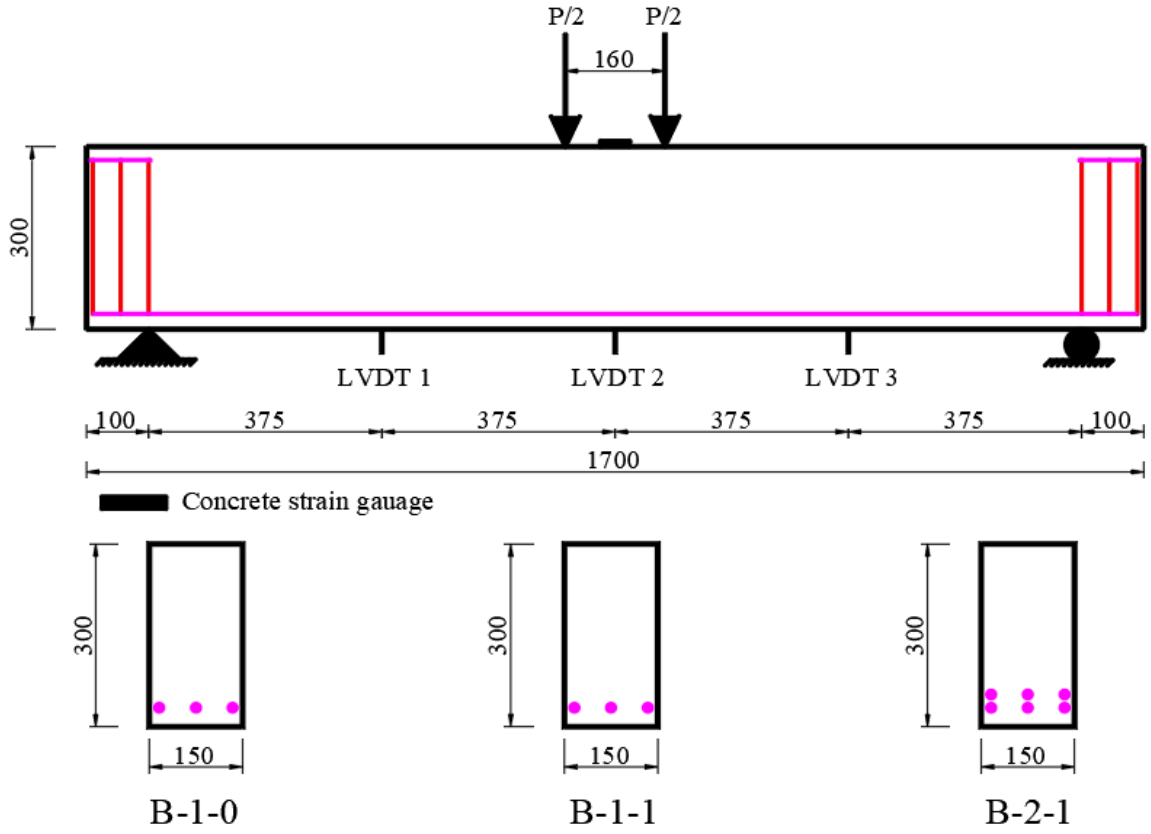

Fig (4): Dimensions, reinforcement details, and strain gauge locations of the test specimens (Note: dimensions in mm).

Table (3): Test matrix and details of the test specimens

ID	Reinforcing Material	$f'c$ (MPa)	ρf (%)	Fire Duration (hr)
B-1-0	GFRP	25	1.0	0.0
B-1-1	GFRP	22	1.0	1.0
B-2-1	GFRP	22	2.3	1.0

Instrumentation

Instrumentation of the beam specimens included three linear variable differential transducers (LVDTs) at different locations for deflection measurement. Two electric strain gauges with a gauge length of 60 mm were bonded to the compression surface of each specimen to measure the compressive concrete strains. Epoxy was used to attach the strain gauges to the compression beam surface after it was cleaned. Fig. 4 illustrates the instrumentation details of the test beams.

Journal of Sustainability and Innovation in Engineering
(IJSIE)
https://www.doi.org/10.56830/IJSIE062023

Fire Exposure System

A steel furnace with seven burners lined parallel to each other was used with dimension 2000 mm × 2000 mm × 600 mm. The furnace was heated to the required temperature, i.e. (500 ◦C) and then kept at this temperature for 2 h. The beams and cylinders were subjected to direct fire. The used regime for cooling the fire beams was air.

Experimental Setup and Testing

The beam specimens were subjected to four-point loading on a clear span length of 1500 mm (see Fig. 4). The beams were supported by two steel plates set on the supports. The load was applied with a 550 kN hydraulic jack in two phases. In the first phase, the load was applied in load-controlled mode at a rate of 2 kN/min up to the first crack. Then, the beam was loaded in load-controlled mode at a rate of 4 kN/min up to failure. The rigid steel beam was used to transfer two equal loads to the specimen. The load was removed from the test beams immediately after reaching the failure load.

Experimental Results and Discussions

Shear Failure Mode and Cracking

The beam specimens clearly failed in shear failure mode before reaching their flexural capacities. Vertical flexural cracks were observed in all specimens perpendicular to the direction of the maximum principal stress induced by pure bending moment in the flexural span zone. Cracking outside the flexural span zone started as the load increased, similarly to flexural cracking. As more load was applied, the shear stress became more dominant and developed curving in both shear spans toward the loading points. Fig. 5 illustrates the typical failure mode of the tested beam specimens.

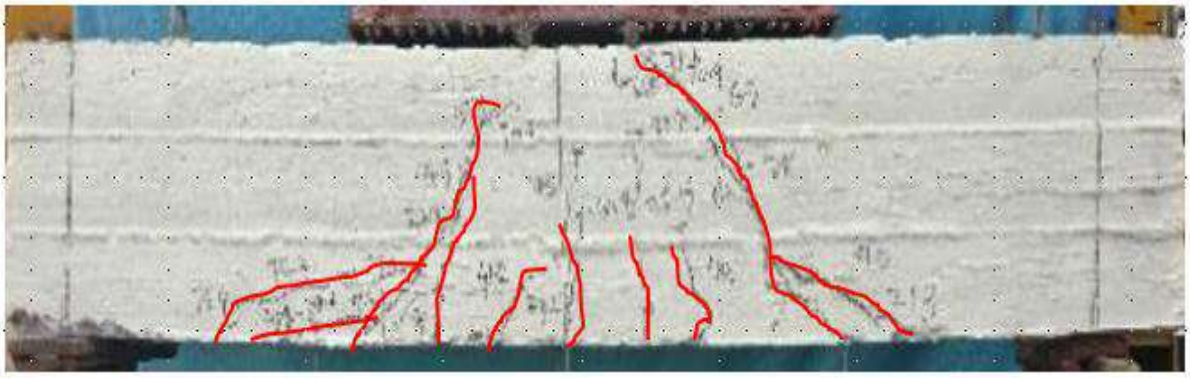

Fig (5): Typical crack pattern of beams

Journal of Sustainability and Innovation in Engineering
(IJSIE)
https://www.doi.org/10.56830/IJSIE062023

Load–Deflection Behavior

This section presents the load–deflection curves of the test specimens in two groups to show the effect of test parameters on shear behavior, as shown in Figures 6 and 7. It can be observed that the relationship of load-deflection was bilinear. The first stage of the load-deflection curve for all beams exhibited a linear response until reaching flexural cracking. The second stage, after cracking, all specimens showed a significant loss of stiffness with a considerable increase in their point loads deflections. As shown in Fig. 6, the decreased stiffness varied because of the different reinforcement ratios. It can be noticed that increasing the reinforcement ratio resulted in higher stiffness and decreased its deflection at all stages of loading.

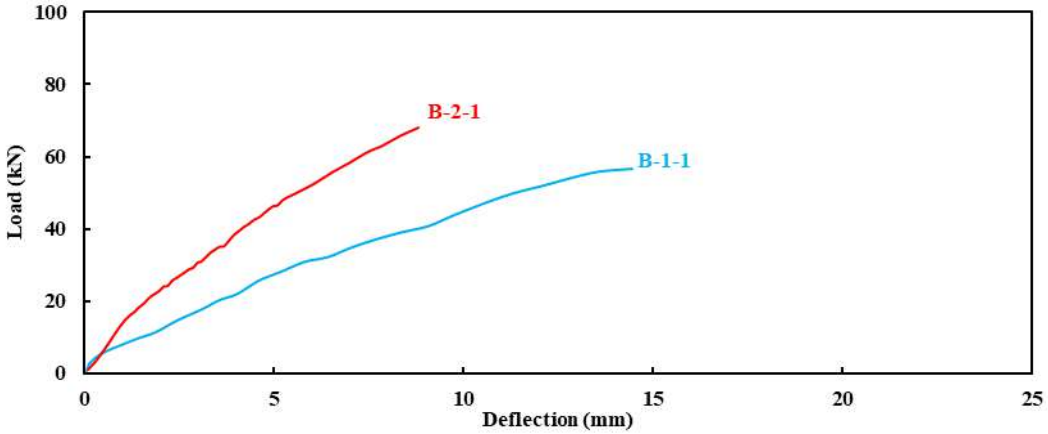

Fig (6): Load–deflection curves for beams at the same temprature (500 ◦C).

Fig. 7 shows that the stiffness of the RC beams decreased when the beams are exposed to fire at the same reinforcement ratio. In other words, B-1-0 was stiffer than B-1-1 at the same reinforcement ratio (1.0 %). In addition, the shear strength of the beam exposed to fire is 88 % of its room temperature shear strength.

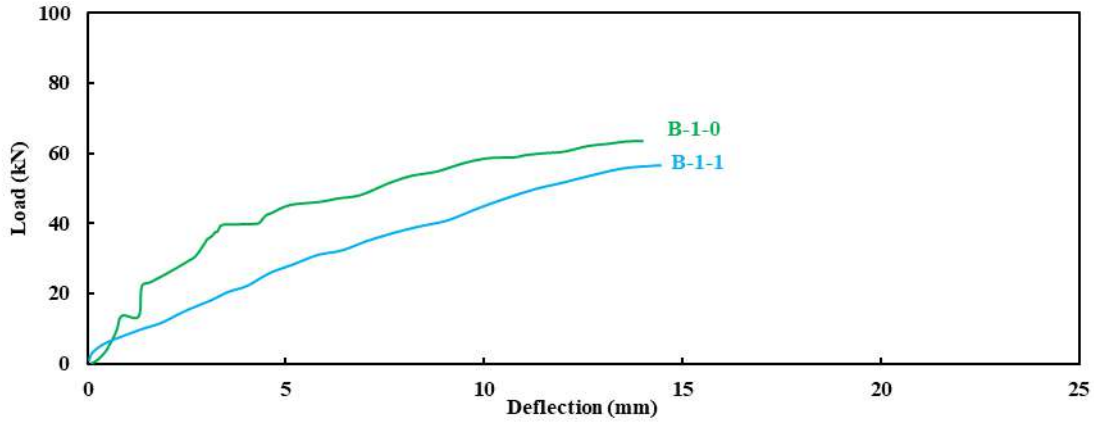

Fig (7): Load–deflection curves for beams at the same reinforcement ratio (1.0%).

Journal of Sustainability and Innovation in Engineering
(IJSIE)
https://www.doi.org/10.56830/IJSIE062023

Effect of the GFRP longitudinal reinforcement ratio

Fig. 8 shows the influence of reinforcement ratio of the GFRP bars on the shear strength of the RC beams. The vertical axis represents the experimental load of the tested beams. While the horizontal axis represents the reinforcement ratio ρ. It was found that the shear strength increased as the reinforcement ratio was increased. The shear strength increased by 13.0 % when the longitudinal reinforcement ratio increased by 130 % (from 1.0 to 2.3 %). Moreover, cracking pattern for beams with higher amount of longitudinal reinforcement was more observed than that for beams with lower amount of longitudinal reinforcement.

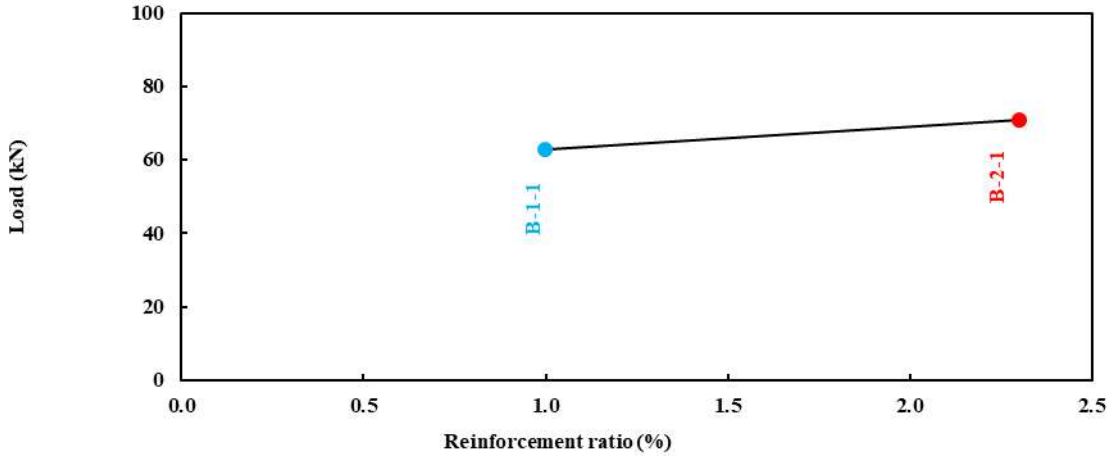

Fig (8): Experimental load versus reinforcement ratio for GFRP reinforced beams.

Conclusions

This paper presents the results of a research program to investigate the shear behavior of GFRP RC beams exposed to severe fires. The main remarks from the study can be drawn as follow:

1. Diagonal tension failure was the dominant failure mode of the GFRP RC beam specimens.
2. Increasing the reinforcement ratio resulted in higher stiffness and decreased its deflection at all stages of loading. The shear strength increased by 13.0 % when the longitudinal reinforcement ratio increased by 130 % (from 1.0 to 2.3 %).
3. The shear strength of the beam exposed to fire is 88 % of its room temperature shear strength at the same reinforcement ratio.
4. It is recommended to extend this study with more experimental works considering more samples to be tested for each test parameters.

Acknowledgment

The authors thank the technical staff of the structural laboratory in the Department of Civil Engineering at Helwan University.

References

ACI, 4.-0. (2004). Guide test methods for fiber-reinforced polymers (FRPs) for reinforcing or strengthening concrete structures, ACI Committee 440. *American Concrete Institute, Farmington Hills, Michigan, USA*.

American, C. I. (2015). Guide for the design and construction of concrete reinforced with FRP bars. *ACI 440.1R-15, Farmington Hills, MI*.

ASCE-ACI, C. 4. (1998). Recent approaches to shear design of structures. *J. Struct. Eng., 10.1061/ (ASCE) 0733-9445(1998)124:12(1375)*, 1375–1417.

ASTM, D. (2011). Tensile properties of fiber reinforced polymer matrix composite bars. *ASTM International, West Conshohocken, PA*.

ASTM. (2015). Standard test methods for fire tests of building construction and materials. ASTM E119. *West Conshohocken, PA: ASTM*.

C39/C39M-18., A. (2018). Standard test method for compressive strength of cylindrical concrete specimens. *ASTM International, West Conshohocken, PA*.

Canadian, S. A. (2019). Canadian highway bridge design code. *CSA S6-19, Rexdale, Ontario, Canada*.

CSA, C. S. (2012). – Re-approved in 2017 –. Design and construction of building components with fiber reinforced polymers. *CSA S806-12. Rexdale, Ontario, Canada*.

Gooranorimi, O., Claure, G., De Caso, F., Suaris, W., & Nanni, A. (2018). Post-fire behavior of GFRP bars and GFRP-RC slabs. *Journal of Materials in Civil Engineering, 30(3)*, 04017296.

Hajiloo, H., Green, M. F., Noël, M., Bénichou, N., & Sultan, M. (2019). GFRP-reinforced concrete slabs: fire resistance and design efficiency. *Journal of Composites for Construction, 23(2)*, 04019009.

Hajiloo, H., Green, M. F., Noël, M., Bénichou, N., & Sultan., M. (2017). Fire tests on full-scale FRP reinforced concrete slabs. *Compos. Struct. 179*, 705–719.

Hajiloo, H.; Green, M. F.; Noël, M.; Bénichou, N.; Sultan, M. (2019). GFRP-reinforced concrete slabs: fire resistance and design efficiency. *Journal of Composites for Construction, 23(2)*, 04019009.

MacGregor, J. G., & Wight, J. K. (2005). Reinforced concrete: Mechanics and design. 4th Ed. *Prentice-Hall, Upper Saddle River, NJ*.

Nigro, E., G. Cefarelli, A., Bilotta, G. M., & Cosenza, E. (2011). Fire resistance of concrete slabs reinforced with FRP bars. Part I: Experimental investigations on the mechanical behavior. *Composites Part B 42 (6)*, 1739–1750.

International Journal of Sustainability and Innovation in Engineering (IJSIE)
https://www.doi.org/10.56830/IJSIE062023

Analyzing the Nonlinear Finite Element Behavior of FRP Composite Electrical Structures in Flexural Loading

https://www.doi.org/10.56830/IJSIE06202304

Hamdy Mohamed
Department of Civil Engineering, Université de Sherbrooke, Sherbrooke, Quebec, Canada, J1K 2R1

Abstract:

Finite Element Analysis of Flexural Behavior in Full-scale Tapered FRP Pole Structures: Influence of Fiber Orientations, Circumferential Layers, and Carbon Fiber Substitution. In this study, we present a finite element modeling analysis of the nonlinear behavior of laterally loaded full-scale tapered fiber-reinforced polymer (FRP) pole structures. The study explores the impact of various parameters, including fiber orientations in longitudinal and circumferential layers, the number of circumferential layers, and the substitution of glass fiber with carbon fiber in the FRP pole compositions.

The FRP poles in question were manufactured using the filament winding technique, with E-glass fiber and epoxy resin as the primary materials. Our analysis results exhibit a significant correlation between the finite element analysis and experimental data, emphasizing the critical role of fiber orientation in determining flexural behavior.

The findings underscore the advantages of incorporating circumferential layers and highlight that enhanced strength can be achieved by incorporating both outer and inner circumferential layers alongside longitudinal layers. Moreover, substituting carbon fiber for glass fiber in the FRP poles results in notable improvements, with increased total load capacity and stiffness as the percentage of carbon fibers rises.

1. Introduction

In recent years, FRP composites, which are made of reinforcing fibres and a thermosetting resin, have been widely used as advanced construction materials. FRP provide several advantages over traditional construction materials (steel, concrete, wood): high strength to weight ratio, high stiffness, resistance to corrosion, ease of installation and high durability (Fujikake, Mindess, & Xu, 2004). Therefore, the tapered FRP poles are currently considered attractive in the application of the light poles and electrical transmission tower element.

There is a lack to study the behaviour of the hollow tapered FRP pole structures. These due to the limited number of experimental and theoretical studies, which have been conducted on the behaviour of the tapered GFRP poles structure under lateral load (Li, 1996); (Crozier, Dussel, Bushey, & West, 1995); (Derrick, 1996);

(Ibrahim, Polyzois, & Hassan, 2000); (Ibrahim & Polyzois, "Ovalization analysis of fiber reinforced plastic poles", 1999). The most of these studies were established on the behaviour of the FRP poles without service opening. The existence of service opening in the FRP poles, reduce the strength at the location of this opening, due to small thickness-to-radius ratio, ovalization and local buckling behaviour of the FRP poles. Therefore the part which includes this hole must be addressed and finding the optimum geometrical details for it to be compatible with the upper and lower zones over the length of the pole to attain the required total capacity under lateral loads.

The finite element analysis is a good way that can be used to simulate and predict the actual behaviour of FRP poles. A theoretical analysis by finite element method were developed for the analysis of FRP hollow tapered poles, to perform a linear static analysis, linear buckling analysis, linear *P-Δ* analysis, a geometrical nonlinear analysis of beam-column-type bending and an ovalization analysis (ZM., 1995). Extensive numerical results were presented showing the effect of different lamination and geometric parameters of the multilayered composite cylinder on the accuracy of the static and vibrational responses (Noor, Sctt, & Peters, 1991). The Brazier's theory for the nonlinear collapse of isotropic circular cylinders had been extended by Long-yuan 1996 to predict the instability critical loads of orthotropic composite tubes under pure bending by simple formulations. The formulations were based on the assumption that the instability of an orthotropic composite tubes under pure bending is due to the ovalization of its cross section.

In this paper, the finite element program was used to perform a nonlinear numerical analysis for 10566 mm (35 ft) tapered glass fibre-reinforced polymer (GFRP) poles with service opening, under lateral load to present the wind load on the structure. The model was performed to simulate the actual behaviour of the static test according to the recommendations described in ASTM and ANSI standard. A parametric study was carried out to study the effect of longitudinal and circumferential angle orientation of the fibre, number of circumferential layers and the effect of replacing glass fibre by carbon fibre on the FRP pole behaviours. The ultimate capacity, top deflection and stiffness increase are presented.

2. Finite Element Analysis

A nonlinear finite element model of FRP poles was developed using the commercial software ADINA finite element program. The finite element method used to analyze and simulate the behaviours of GFRP poles. Large deflection was included in the analysis and appropriate failure criteria were used in determining the failure load. The finite element analysis was verified through comparison with the available

experimental data obtained from the static testing of full-scale specimens, according to the recommendations described in ASTM and ANSI standard.

The following sections present the major features of the finite element method used in this paper:

2.1. Geometrical Modeling

The specimens were tapered hollow sections, 10566 mm in length. The inner diameters at the base and at the top were 270.00 and 114.00 mm, respectively. The specimen divided through the height into three zones, I, II and III, The 101.6 x 304.8 mm-(width x length) service opening is located at the center of the middle zone II and was in the compression side. The typical specimen dimension, cross section and details of the three zones, are shown in Figure. 1. GFRP poles are fabricated using filament winding technique, different fibre angles with respect to the longitudinal axis of the pole were used: (90°, ±10°) at the bottom zone I, (90°, ±45°, ±10°) at the middle zone II and (90°, ±10°) at the top zone III. The layer thickness is 0.432 mm. The pole modeled with total number of elements 2256 (16 and 141 in the circumference and longitudinal direction, respectively), the mesh layout were fine in the bottom area of the maximum stress and expected failure zone, and gradually becomes coarse at the top, this was made by the automatic mesh density option of the program. The general layout of the mesh distribution and the used finite element models are shown in Figure. 2.

The under ground length of the GFRP poles were restraint along two opposite half circumference area, the first area at the end of the base and the second area at the ground line.. Each node along the supported area was restrained against the vertical (in z-direction), the horizontal (in x and y directions) movements. This Configuration of restraints was to simulate the support condition described in standards ASTM D 4923-01 and ANSI C 136.20-2005 for measuring the Load- deflection behaviour of FRP poles, see Figure. 3.

2.2. Composite Shell Elements

An eight-node quadrilateral multilayered shell element was used in the model. Each node has six degrees of freedom, three translations (Ux, Uy, and Uz) and three rotations (Rx, Ry, and Rz). The composite shell elements are kinematically formulated in the same way as the single layer shell elements, but an arbitrary N number of layers can be used to make up the total thickness of the shell. Layers are numbered in sequential order starting from 1 at the bottom of the shell (ADINA., 2006).

Newton-Cotes with high order of 5×5 numerical integration was used for the evaluation of the element matrices in the r-s plane of the shell element, to avoid

International Journal of Sustainability and Innovation in Engineering
(IJSIE)
https://www.doi.org/10.56830/IJSIE062023

spurious zero energy. 3-point Newton-Cotes numerical integration was used through the shell thickness to obtain an accurate profile of the transverse shear stress.

The material model which be used with the shell element is elastic-orthotropic with large displacement /small strain. In the large displacement formulation/small strain formulation, the displacement and rotation can be large, but the strains were assumed to be small. Orthotropic material properties in the fibre and transverse to the fibre direction were defined. Fibre orientation for each layer was specified by defining the fibre angle with respect to the element axes.

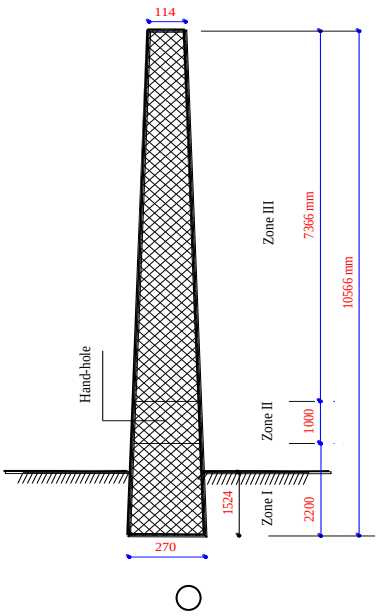

Figure 1. Dimension of full-scale FRP pole

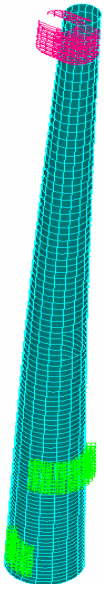

Figure 2. Finite element mesh

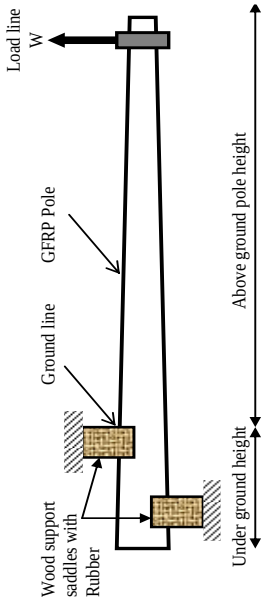

Figure 3. Specified methods for testing FRP poles

2.3. Macroscopic Failure Criteria

The mechanical behaviour of advanced fibre reinforced composite materials is topic which has attracted a great deal of interest in recent years. Failure criteria have been developed to predict the materials strength properties of the orthotropic composite materials. Composite materials are anisotropic (properties vary depending on the direction in which they are measured); hence the strength properties of fibre-reinforced materials are strongly dependent on the direction of loading. Accordingly, more than one parameter is needed. The Tsai-Wu failure criteria are provided in ADINA for the analysis of shell structures using the elastic-orthotropic material models. This failure theory expands the Tsai-Hill criteria by including linear terms which characterize the different strength in tension and compression and quadratic terms. This criterion provides an ellipsoid shaped failure envelope in the stress space.

International Journal of Sustainability and Innovation in Engineering
(IJSIE)
https://www.doi.org/10.56830/IJSIE062023

2.4. Loading

The FRP pole was subjected to a horizontal pressure load (W) below the top of the pole edge by 300 mm according to the ANS C 136.20-2005. The value of (W) was varied from zero to the ultimate load capacity corresponding to each pole. The pole was incrementally loaded using 100-150 time steps. This variation is automatically done by the AUI according to the condition of convergence. To avoid local failure under the applied load, the load had been distributed over circumferences area to simulate the same effect of the experimental load.

3. Material Properties

The material properties for both the fibre and the resin are presented in Table 1. The mechanical properties of the FRP laminate were obtained from the material properties of the E-glass fibre and the epoxy resin. They used to calculate the effective modules of elasticity of the orthotropic material based on micromechanical models. The Rule of Mixture was used to evaluate the modulus of elasticity in the fibre direction (E_l), and the major Poisson's ratio (υ_{12}) as follows (Adams, 1987):

$$[1]\quad E_1 = E_f \mu_f + E_m \mu_m$$

$$[2]\quad \upsilon_{12} = \upsilon_f \mu_f + \upsilon_m \mu_m$$

Where,

μ_f and μ_m are the fibre and the matrix volume ratios, respectively;
E_f and E_m are the fibre and the matrix Young's modules, respectively; and
υ_f and υ_m are the fibre and the matrix Poisson's ratios respectively.

equations given by (Gay, 1989) were used to calculate the effective Young's modulus in the transverse direction (E_2) and the shear modulus (G_{12}), by using the fibre and matrix properties (E_2) and (G_{12}) were derived as follow:

$$[3]\quad E_2 = \frac{1}{\left[\frac{\mu_f}{E_f} + \frac{\mu_m}{E_m}\right]}$$

$$[4]\quad G_{12} = \frac{1}{\left[\frac{\mu_f}{G_f} + \frac{\mu_m}{G_m}\right]}$$

Where,
G_f and G_m are the fibre and the matrix shear modules, respectively.

Table 1: Properties of E-Glass and matrix:

	Fibres	
	E-Glass	Carbon
Tensile modulus(MPa)	80 000	250 000
Shear modulus(Mpa)	30 000	93 750
Poisson's ratio	0.25	0.20
	Epoxy resin Araldite GY 6010	
Density (Kg / m^3)	1200	
Tensile modulus(Mpa)	3380	
Shear modulus(Mpa)	1600	
Poisson's ratio	0.4	

International Journal of Sustainability and Innovation in Engineering
(IJSIE)
https://www.doi.org/10.56830/IJSIE062023

4. Results and Discussion

Failure of the modeled FRP poles was determined when the divergence of the solution was achieved or when the Tsai-Wu failure criterion value reached unity. A comparison between the finite element analysis and the results obtained from experimental testing of full-scale prototypes, was in terms of the load-deflection relationship and the ultimate load carrying capacity. Figure. 4 represent the load deflection relationship for the experimental and finite element analysis for 20 and 35 ft height GFRP poles. It is evident from this figure that there is a strong correlation between the results obtained from the finite element analysis and the experimental results. The 35 ft GFRP pole failed at the ground level due to the local buckling and before this failure distortion of cross section at service opening location was occurred, (see Figure. 5).

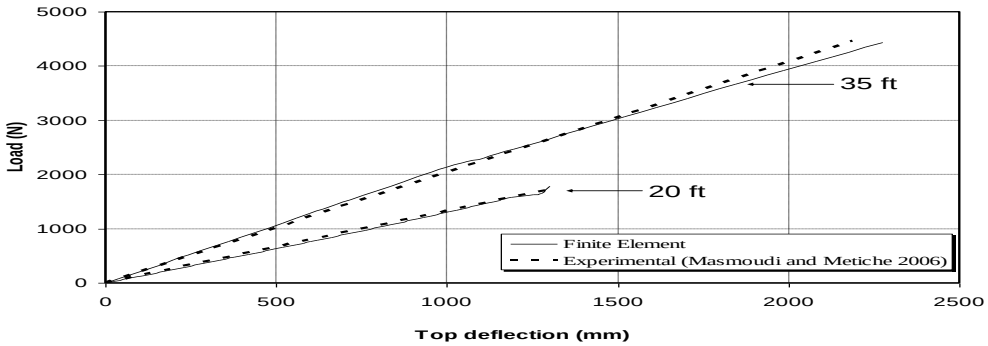

Figure 4. Comparison between experimental and FE load-deflection relationship for

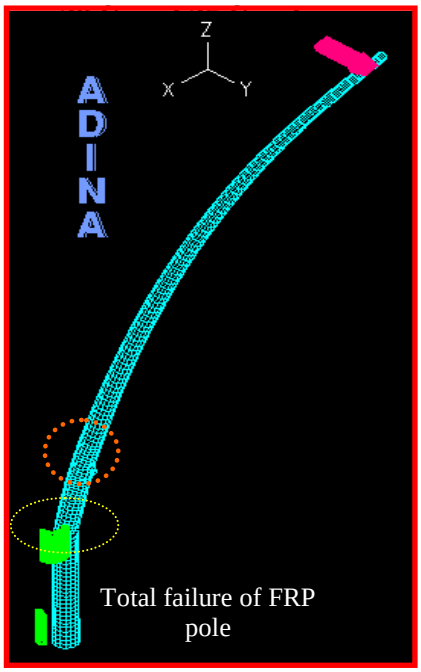

Figure 5. Deformed shape for 35 GFRP pole at failure

Parametric Study

International Journal of Sustainability and Innovation in Engineering
(IJSIE)
https://www.doi.org/10.56830/IJSIE062023

Based on the agreement of the finite element analysis, the effects of the following parameters were carried out to better understand the flexural behaviour of FRP poles:

1- fibre orientations of longitudinal layers
2- fibre orientations of circumferential layers
3- number of circumferential layers, and
4- replacing glass fibre by carbon fibre.

The same finite element analysis was used to extend the study and examine these parameters effect of longitudinal and circumferential angle orientation of the fibre, number of circumferential layers and the effect of replacing glass fibre by carbon fibre on the FRP pole behaviours, with the same details of wall thickness, dimension of the GFRP pole (35 ft) and material properties. Table 2 shows the stacking sequence and fibre orientation for 7 prototypes models to study the effect of the first, second and third parameters. P_o was taken the reference. P-1 and P-2 are proposed to study the effect of fibre orientations of longitudinal layers, by changing the fibre orientation from ±10 to ±20 and ±30 degree for P-1 and P-2, respectively. P-3 and P-4 are proposed to study the effect of fibre orientations of circumferential layers, by changing the fibre orientation from ±90 to ±70 and ±50 degree for P-3 and P-4, respectively. P-5 and P-6 are proposed to study the effect of number of circumferential layers, by changing the fibre orientation from ±90 to ±10 for P-5, it is meaning that this model has not any circumferential layers. Finally in P-6, the number of circumferential layers was assumed to increase for 4 layers.

A parametric study had been made to investigate the effect of the percentage of replacing glass fibre by carbon fibre on the FRP pole behaviours. To study this parameter, 7 prototypes were defined in ADINA program. Each prototype redefined by replacing one or two or three or four galas fibre layers by carbon fibre. These layers were changed in the circumferential and/or longitudinal by alternative. Table 3 shows the stacking sequence, numbers, type and percentage of carbon fibres for each model.

Table 2: Stacking sequence and fibre orientation of layers

Pole model Id	Zone I, III	Zone II	Parameters		
P_o	$[90, (\pm10)_5, 90]$	$\{90, \pm45\ [90, (\pm10)_5, 90]\ \pm45, 90\}$	1	2	3
P-1	$[90, (\pm20)_5, 90]$	$\{90, \pm45\ [90, (\pm20)_5, 90]\ \pm45, 90\}$		1	
P-2	$[90, (\pm30)_5, 90]$	$\{90, \pm45\ [90, (\pm30)_5, 90]\ \pm45, 90\}$		1	
P-3	$[70, (\pm10)_5, 70]$	$\{70, \pm45\ [70, (\pm10)_5, 70]\ \pm45, 70\}$		2	
P-4	$[50, (\pm10)_5, 50]$	$\{50, \pm45\ [50, (\pm10)_5, 50]\ \pm45, 50\}$		2	
P-5	$[10, (\pm10)_5, 10]$	$\{10, \pm45\ [10, (\pm10)_5, 10]\ \pm45, 10\}$		2	
P-6	$[90_2, (\pm10)_4, 90_2]$	$\{90, \pm45\ [90, (\pm10)_4, 90]\ \pm45, 90\}$		3	

International Journal of Sustainability and Innovation in Engineering
(IJSIE)
https://www.doi.org/10.56830/IJSIE062023

Table 3. Stacking sequences and percentage of carbon fibres in different prototype.

Proto. Id.	Stacking sequences	Number of carbon fibre layers	Parameters	Percentage of carbon fibres %
P_o	[90, $(\pm10)_5$, 90]	0	4	0
2	[90, 10, $(\pm10)_4$, -10, 90]	1 circumferential	4	8.00
3	[90, 10, $(\pm10)_4$, -10, 90]	1 longitudinal	4	8.00
4	[90, 10, $(\pm10)_4$, -10, 90]	2 circumferential	4	16.00
5	[90, 10, $(\pm10)_4$, -10, 90]	2 longitudinal	4	16.00
6	[90, 10, $(\pm10)_4$, -10, 90]	2 circ and 2 long	4	32.00
7	[90, ±10, $(\pm10)_3$, ±10, 90]	4 longitudinal	4	32.00

The under line layers indicate to carbon fibre layers

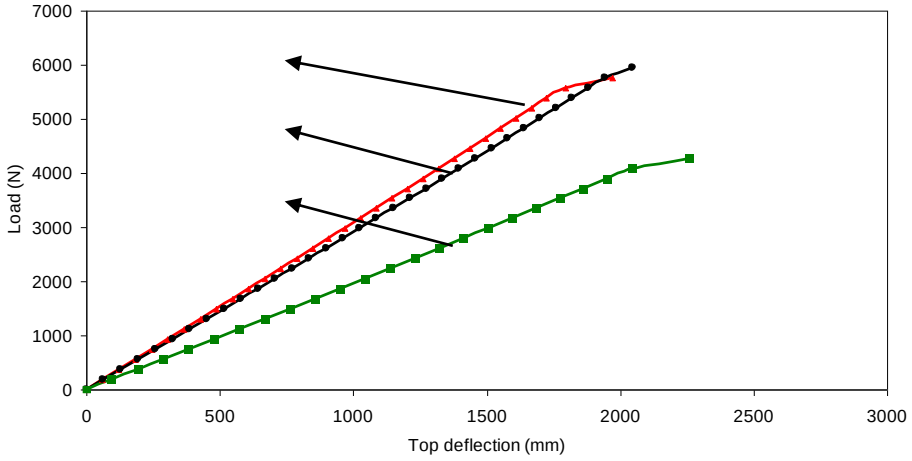

Figure 6. Effect of fibre orientations of longitudinal layers on load deflection relationship

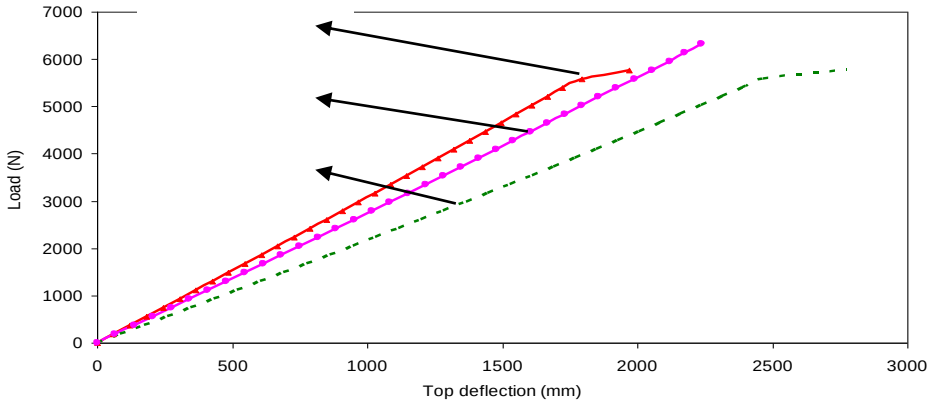

Figure 7. Effect of fibre orientation of circumferential layers on load deflection relationship

International Journal of Sustainability and Innovation in Engineering
(IJSIE)
https://www.doi.org/10.56830/IJSIE062023

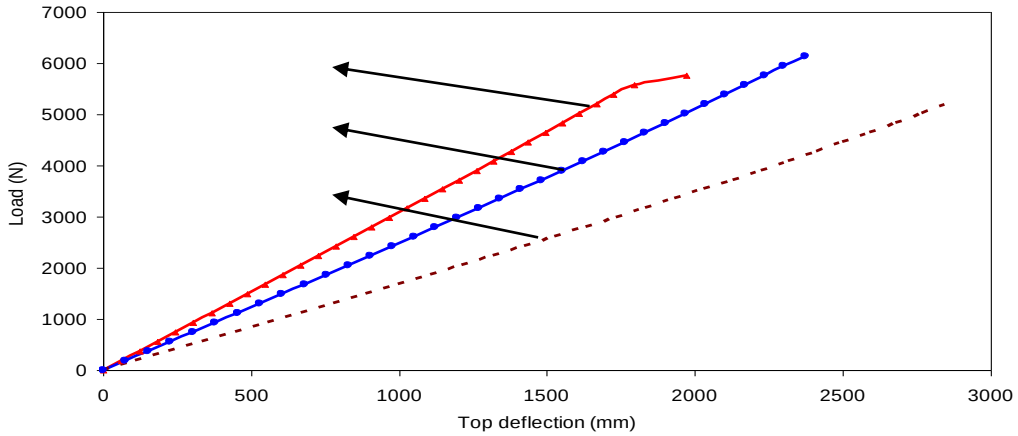

Figure 8. Effect of number of circumferential layers on load deflection relationship

The load deflection relationships are plotted for the numerical results of the different models in figures 6, 7, 8 and 9. It is observed that increasing the fibre orientations of the longitudinal layer a significant droop in the failure load and an increase of the deflection at all load level was occurred as shown in Figure. 6. Also decreasing the fibre orientation of the circumferential layers from 90 to 70 and then 50 degree the load decreased and deflection increased as shown in Figure. 7. It is cleared from Figure. 8 that the importance of the inner and the outer circumferential layers with the longitudinal layers for the FRP poles. This is evident from the result of the model P-5, it hadn't any circumferential layer and a significant droop in the failure load and an increase of the deflection at all load level was occurred.

Table 4. Results of the finite element analysis for replacing glass fibre by carbon fibre.

Proto. *Id.*	Number of carbon fibre layers	Percentage of carbon fibres %	Failure load (FL) (kN)	Max Deflection (mm)	Stiffness (St) (N/mm)
P_o	0	0	**5.58**	1800	**3.10**
2	1 circumferential	8.00	**6.30**	1730	**3.64**
3	1 longitudinal	8.00	**6.14**	1660	**3.69**
4	2 circumferential	16.00	**6.42**	1650	**3.67**
5	2 longitudinal	16.00	**6.14**	1360	**4.5**
6	2 circ and 2 long	32.00	**7.11**	1380	**5.15**
7	4 longitudinal	32.00	**7.53**	1450	**5.19**

International Journal of Sustainability and Innovation in Engineering
(IJSIE)
https://www.doi.org/10.56830/IJSIE062023

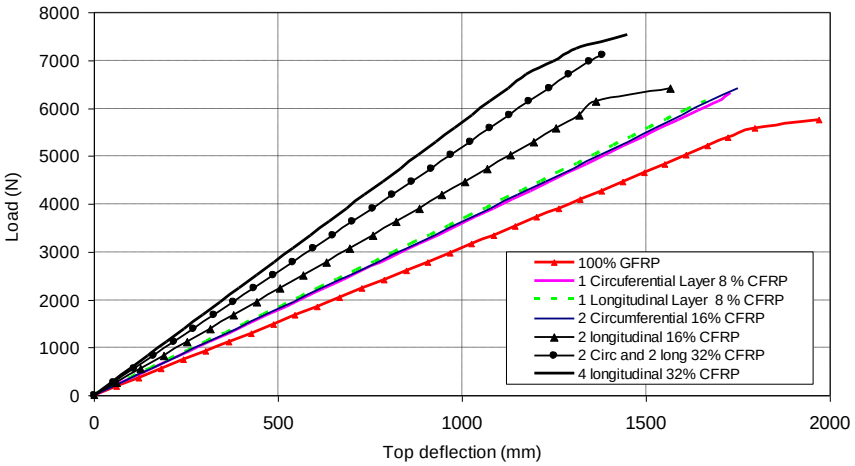

Figure 9. Effect of incorporating carbon fibre on load deflection relationship.

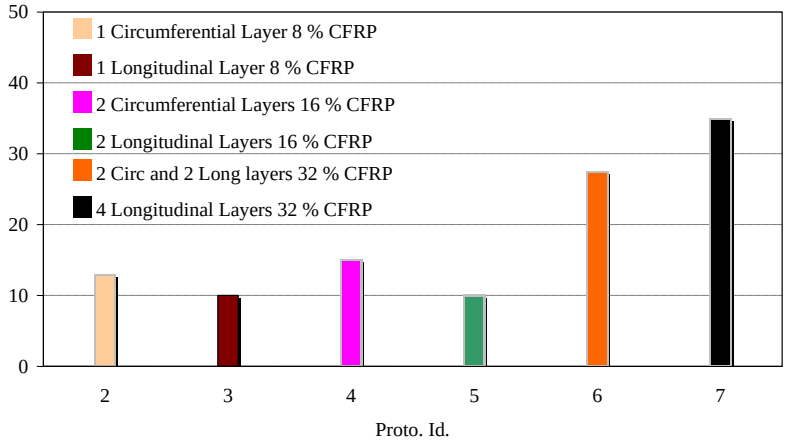

Figure 10. Effect of incorporating carbon fibre on failure load of FRP poles

$$\% \text{ Failure Load increase} = \frac{FL_i - FLp_o}{FLp_o} \times 100,$$

FL_i= failure load for different prototype 2 or 3,……..,7

Table (4) shows the failure load, the deflections, and the stiffness factor of the FRP poles for different prototypes for replacing glass fibre by carbon fibre. Fig. 9 shows the effect of incorporating carbon fibre on load deflection relationship with different percentage of carbon fibres. Figure. 10 shows the effect of incorporating carbon fibre on the percentage increase of the failure load of the FRP poles. Also Figure. 11 shows the effect of incorporating carbon fibre on the percentage increase of the stiffness of the FRP poles.

It is clear that replacing carbon fibre by glass fibre of the FRP poles a higher improvement in the stiffness and strength was achieved. The total load capacity of the FRP poles and the stiffness were increased with increasing the percentage of

carbon fibre. The percentage increase in ultimate load capacity and stiffness depends on the type of layers. Incorporating longitudinal carbon fibre layers tend to increase the ultimate capacity more than incorporating circumferential carbon fibre layers.

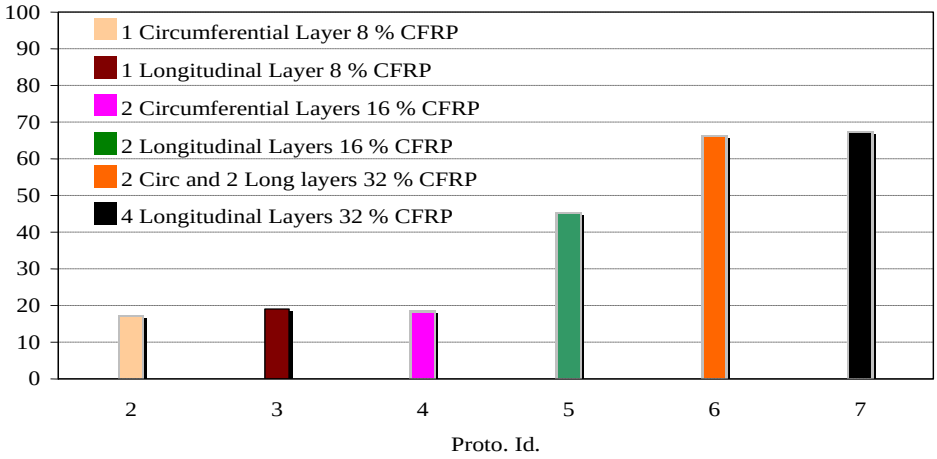

Figure 11. Effect of incorporating carbon fibre on failure load of FRP poles.

$$\% \text{ Stiffness increase} = \frac{St_i - St_1}{St_1} x100$$

St_i = failure load for different prototype 2 or 3,…….,7

5. Conclusions

Finite element analysis is effective for modeling GFRP pole structures. Layered composite shell elements were used in this finite element analysis. The program accounts for the nonlinear behaviour of the poles and includes a strength failure check by applying the Tsai-Wu failure criterion. The results were in an excellent agreement with the experimental results. The finite element method used in this investigation provided an excellent prediction of the critical buckling and material failure loads. The load-deflection curve of GFRP poles under lateral loading is linear up to failure. When the fibre orientation of the longitudinal layer is 10 degree, this yields a higher load capacity with lower deflection. Circumferential layers improve the flexural behaviour of GFRP poles in terms of ultimate load capacity and deflection. The fibre orientation of circumferential layers with 90 degre e for the tapered FRP poles yields higher load capacity and stiffness. The internal and external additional three layers (90, ±45) for the laminate at the middle zone II, improved the flexural behaviour due to the existence of the service opening. The total load capacity of the FRP poles and the stiffness increased with increasing the percentage of carbon fibre.

References

Adams, R. (1987). "Damping properties analysis of composites" Engineering materials handbook. Edited by T.J. Reinhart et al. *ASM International, Materials Park, Ohio, Vol. 1, Composites*, 206–217.

ADINA. (2006). Theory Manual, version 8.4. ADINA R&D. *Inc Wastertown, USA.*

ADINA. 2006. Theory Manual, version 8.4. ADINA R&D, . (n.d.).

Crozier, W., Dussel, J., Bushey, R., & West, J. (1995). "Evaluation of deflection and bending strength characteristics of fibre-reinforced plastic lighting standards". *Department of Transportation, New York, State of California, USA.*

Derrick, G. L. (1996). "Fiberglass Composite Distribution and Transmission Poles", Manufactured Distribution and Transmission Pole Structures Workshop Proceeding, July 25-26. *Eclectic Power Research Institute*, 55-61.

Fujikake, K., Mindess, S., & Xu, H. (2004). "Analytical Model for Concrete Confined with Fiber Reinforced Polymer Composite" . *JOURNAL OF COMPOSITES FOR CONSTRUCTION © ASCE, 8(4)*, 341-351.

Gay, D. (1989). Matériaux composites. *Paris, 2e édition, Hermes.* , p. 485 .

Ibrahim, S., & Polyzois, D. (1999). "Ovalization analysis of fiber reinforced plastic poles". *Composite Structures, 45*, 7–12.

Ibrahim, S., Polyzois, D., & Hassan, S. (2000). "Development of glass fiber reinforced plastic poles for transmission and distribution lines". *Can. J. Civ. Eng. 27*, 850-858.

Li, L. Y. (1996). "Bending Instability of Composite Tubes" . *Journal of Aerospace engineering, 9(2)*, 58-61.

Noor, A. K., Sctt, B. W., & Peters, J. M. (1991). "Assessment of computational models for multilayered composite cylinders" . *Int. J. solids structures. 27(10)*, 1269-1286.

ZM., L. (1995). "Analysis of pole-type structures of fibre-reinforced Plastics by finite element method". *Ph.D. Thesis, University of Manitoba, Winnipeg, Manitoba, Canada.*

International Journal of Sustainability and Innovation in Engineering
(IJSIE)
https://www.doi.org/10.56830/IJSIE062023

PUNCHING SHEAR BEHAVIOR AND STRENGTH OF FLAT SLABS

https://www.doi.org/10.56830/IJSIE06202305

Hamdy Elsayed
Civil Engineering Program, College of Engineering, Applied Science University, Bahrain

Abstract

Prestressed and reinforced concrete flat plates are susceptible to failure due to punching shear. Modeling the punching shear strength of prestressed concrete slabs poses conceptual challenges, as it involves various factors, including the bonding of tendons, stress in tendons during punching failure (which can be indeterminate), tendon banding, and the presence of draped tendons that yield a beneficial vertical component of the prestressing force. Additionally, prestressed concrete slabs typically require supplementary bonded reinforcement.

The objective of this research is to comprehensively investigate the physical behavior of each test specimen, considering parameters such as deflections, crack patterns, crack widths, mode of failure, and to compare the punching shear resistance of interior slab-column connections with various code provisions. The study involved testing a total of five interior slab-column connections, each measuring 1600x1600 mm in size, 80 mm in thickness, with square columns of 180x180 mm and a height of 300 mm.

Keywords: Slab, Punching, Shear, Design, Codes, prestressing.

1. Introduction

Structural system consisting of slabs with uniform thickness supported directly on column without beams is called a flat slab system. Flat slabs are an economical structural system for medium height residential and office buildings. Prestressed concrete flat slabs have additional advantages such as reducing deflection problems and possibility of using larger span - thickness ratios. However, prestressed concrete and reinforced concrete flat slabs are susceptible to failure by punching shear. Punching shear is an undesirable mode of failure in that it occurs without warning and can lead to progressive collapse of large area of slab, or even of complete structures. Punching shear always occurs in regions of large moment, and flexural cracks are observed around the periphery of the loaded area or support. The objective of this paper was to study the following parameter on the behaviour of interior presterssed flat slabs connection:

1- Number of cables in specimens

2- Prestrissing force in slab

2. Building Code Requirements

The code provisions of (ACI, 1989); (ACI-ASCE, 1989); (BS, 1997); CSA A23.3-94, ; (CEB-FIP., 1990), Model code (Comite Euro-International du Beton and Federation international de la Precontraite) are similar in that the punching shear strength of a concrete slab is checked by calculating a nominal shear stress on a control perimeter some fraction of the slab depth away from the column. The mean shear stress acting over this control surface is related usually to the strength of concrete. The existing design procedures and code provisions are based primarily on empirically derived equations that do not necessarily model the mechanism of failure but have been chosen primarily for their simplicity in use and the wide range of conditions over which they produce acceptable results.

The nominal shear capacities of the tested slabs are compared with the nominal shear capacities predicted by the different codes of practice. A detailed account for the provisions of the different codes is given below. The comparison is beneficial for determining the possible conservatism or non-conservatism of some codes.

- **ACI 318 - 02**

ACI- 318-02 specifies that the shear capacity be calculated on the minimum perimeter located at a distance *d*/2 from the periphery of the column or the concentrated load. These provisions follow from the work of ACI-ASCE Committee 423. The punching shear strength around interior columns of two-way prestressed concrete slabs can be predicted by:

$$Vc = 0.083(\beta_p \sqrt{f_{ck}} + 0.3 f_{pc}) b_0 d + V_p \quad (1)$$

- **BS 8110-97**

The British Code used a rectangular control perimeter 1.5*d* from the loaded area for both circular and rectangular loaded areas. For reinforced concrete flat slabs. The available shear force can be calculated from.

$$\frac{V_{eff}}{b_0 d} < V_{CBS} = 0.79\left(100\rho \frac{f_{cu}}{25}\right)^{1/3}\left(\frac{400}{d}\right)^{1/4} < 5.0 < 0.8\sqrt{f_{cu}}\,MPa \quad (2)$$

International Journal of Sustainability and Innovation in Engineering
(IJSIE)
https://www.doi.org/10.56830/IJSIE062023

- **Gardner's method**

(Gardner, 1996) proposed a prediction equation for the punching shear strength of interior slab-column connections of reinforced and prestressed concrete flat slabs, by extending the work of (Shehata & Regan, 1989); (Shehata, 1990), Gardner examined the dependence of the punching shear strength to the concrete strength and the strength for reinforced and prestressed concrete slabs using a control perimeter at the periphery of the loaded area and a (Shehata & Shehata Lidia, 1989) type strength enhancement expression. Columns with circular or rectangular cross sections were analyzed as square columns of the same cross-sectional area. A sensitivity analysis, using the coefficient of variation of the equation coefficient as the criterion of goodness, was used to confirm that the one-third power of concrete strength and steel force was close to optimal. For the unbonded post-tensioned slabs, the prestressed reinforcement ratio was calculated from the initial precompression at the column. i.e., $\rho_p = f_{pc}h/f_{se}d_p$.

The shear force V_d, appropriate to the decompression moment. Was calculated by $V_d \cong 2\pi\rho_p d_p f_{ps}\,(d_p - h/3)$ (developed from the yield line expression for punching shear $V_{yield} = 2\pi M$; M= yield moment per unit width, (Shehata & Shehata Lidia, 1989). This avoids the problem of determining the inclination of the prestressing tendons crossing the failure surface required to calculate the vertical component of the prestressing force. For design purposes the decompression shear force is multiplied by 0.75 to represent the lower 95 percent bound.

$$V_c = 0.55\lambda u d_{eff}\left[1+\left(\frac{250}{h}\right)^{0.5}\right]\left(\frac{h}{4c}\right)^{0.5}\times\left(\frac{\rho f_y d^3+\rho_p f_{ps} d_p^3}{d_{eff}^3}\right)^{1/3}\left[f_{ck}^{(1/3)}\right]+0.75V_d\left[\frac{u}{4c}\right] \quad (3)$$

3. Description of Model Test Specimen

The slab-column connections were tested in this study is one-third scale models. The slab has 160x160-mm side length and 80 mm thickness and is used to represent full-scale flat slab with 9000 mm span and 240 mm thickness. The dimensions were chosen to represent the zone of negative bending moments or lines of contraflexure around an interior column in a prestressed flat plat.

The materials used in this work were locally produced ordinary Portland cement, natural aggregates and tap drinking water. The compressive strength, setting times, expansion and fineness of cement satisfied the requirements of the Egyptian standard specifications. Graded crushed natural dolomite stone of maximum nominal size of 20 mm had been used as a coarse aggregates and natural

siliceous sand had been used as fine aggregates. The ratio between coarse and fine aggregates used in this work was 2:1. The cement content was 350 kg/m^3 and W/C ratio was 0.5.

Dry components (gravel, sand and cement) were firstly mixed mechanically for one minute to ensure uniformity of the mix. Then water is added and mixed thoroughly. As soon as mixing completed,, concrete is cast in the forms and moulds and then compacted by using standard methods. The forms were designed in such a way to ensure water tightness and easy stripping. After 7 days all specimens were removed from moulds, and cured for 28 days. The resulted compressive strength of the produced concrete was between 300 and 320 kg/cm^2.

4. Test setup and Loading Frame

The loading frame of the structural and materials testing laboratory was applying monotonically increasing vertical static load. The slab was simply supported on four sides, resting on strips of neoprene rubber of 80-cm width and 15 mm thickness placed on the center of the flange of the supporting steel beam (See Fig 1).

The loading frame consists mainly of the following parts:

- Three I-beam fixed at right angle and fixed by angles and bolts.
- A small I-beam fixed vertically to horizontal I-beam on the floor to rest dial gauges.

The force was applied on to the column using a hydraulic jack of 250 kN capacities. The loading parts consist of two plates having dimension 300x300 mm and 20 mm thick placed at a distance 500 mm from the c.g of column to achieve uniform loading along all column width. The load cell, which was connected to the digital reading device, was placed on top of the upper plate.

5. Measuring Devices

5.1. Deflection

Dial gauges with an accuracy of 1/100 mm and total displacement of 50 mm were used for deflection measurements at the top face of the slabs. Four dial gauges were fixed at the level of the top of steel beam fixed at the right of the loading frame to measure the deflection of the slab.

International Journal of Sustainability and Innovation in Engineering
(IJSIE)
https://www.doi.org/10.56830/IJSIE062023

5.2. Strain measurements

Strain gauges type KFG-5-120-C1-11 of 5-mm length was used to measure the strains on the strand in two directions and flexural reinforcement. For each slab, the electrical strain gauges were connected to a strain reading device. The accuracy of the strain indicator is 1x10-6. The locations of the strain gauges are shown in Figs 2. (a, b, c, d). Two-strain gauge were at the face of column in the tension side of reinforcement, one was at distance 50 mm from the column face and one at 150 mm from the face of column. Two strain gauges wear connected with the strands in each direction; one was in middle strand at distance 50 mm from column in two directions. And one in anther strand which beyond the middle strand in two direction. The steel and strand strain was measured and recorded using strain indicator connector connected to the strain gauge by wires and the reading were taken at each increment of loading.

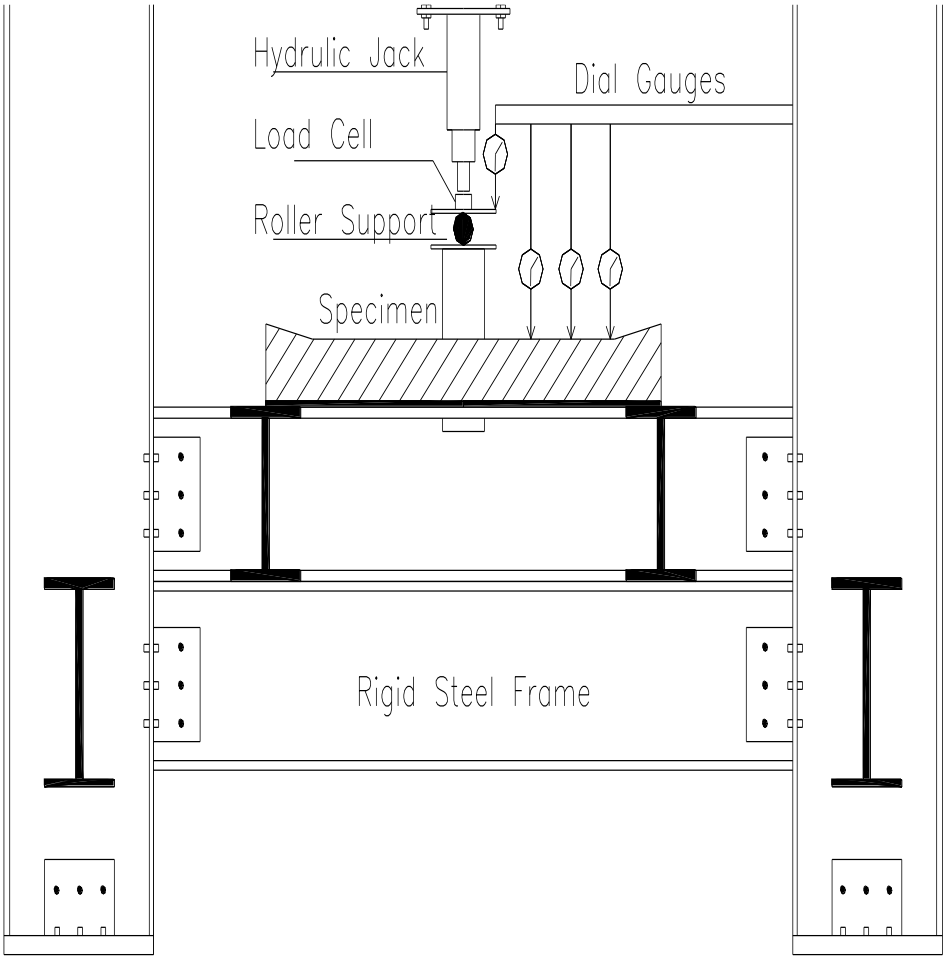

Fig 1: Test set up

International Journal of Sustainability and Innovation in Engineering
(IJSIE)
https://www.doi.org/10.56830/IJSIE062023

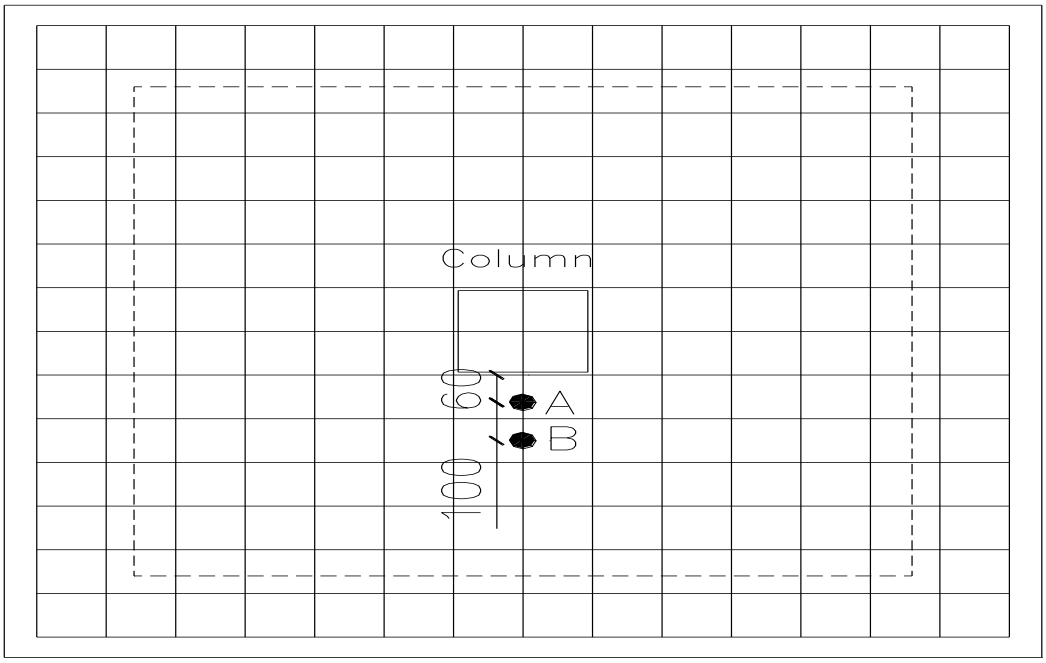

Fig.2. Strain gauge location

6. Test program

The parameters, which were studied experimentally in this research, Number of cables in specimens Prestressing force in slab. The details of test specimens are listed in table (1) and divided, as mentioned before to two groups. Group No 1, It consists of three prestressed flat slabs (P.F.S1, P.F.S2, P.F.S9) to study the effect of number of cables on behavior of slab , these specimens contain (3 , 4 , 5) cables respectively in two direction. The total prestressing force is constant for these entire specimens equal 3.82 kN in each direction. Group No 2, It consists of two prestressed flat slabs (P.F.S2, P.F.S6) to study the effect of prestressing force value on behavior of slab , it consist of four cables in each direction .The prestressing force for slab (P.F.S2) and (P.F.S6) are 3.82 kN, 5.00 kN respectively in each direction.

Table 1: Description of Test Specimens

Group No	Parameter Effect	Slab No	Number of cables	Presstrising Force kN	Top and bottom steel
1	Number of cables	P.F.S1	3	3.82	14 ϕ 6
		P.F.S2	4	3.82	14 ϕ 6
		P.F.S9	5	3.82	14 ϕ 6
2	Presstresing force	P.F.S2	4	3.82	14 ϕ 6
		P.F.S6	4	5.00	14 ϕ 6

International Journal of Sustainability and Innovation in Engineering
(IJSIE)
https://www.doi.org/10.56830/IJSIE062023

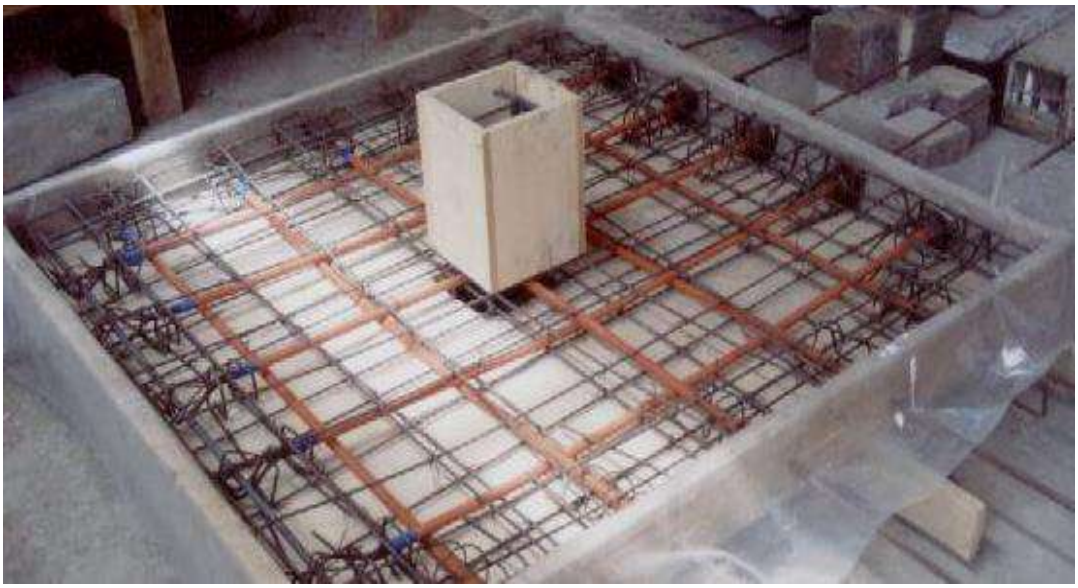

Fig.3: Over view of preparation for slabs

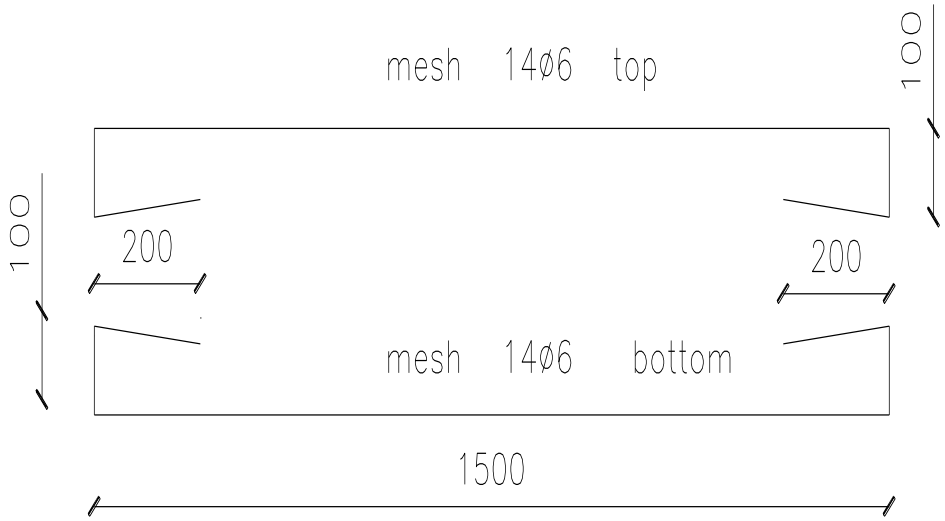

Fig.4. Details of reinforcement for all prestressed slabs

7. Test results and analysis

All specimens exhibited similar cracking behaviour throughout the test, and failed in a combination of flexure and shear with a final failure mode of "Punching shear ". After failure all specimens remained supported by the tendons, passing through the column and aided by the bonded reinforcement. Each specimen remained intact after failure, and did not completely collapse. Cracking and failure loads are tabulated in Table 2. The measured deflections at column face for all tested slabs are plotted in Fig. 5. The measured steel strains and strand strains are plotted in Figs. 6.

International Journal of Sustainability and Innovation in Engineering
(IJSIE)
https://www.doi.org/10.56830/IJSIE062023

7.1 Strains

Steel Strain The profiles of the measured strains with loading are plotted in Figs .6. (a, c, e, g). Fig .6. (a) Shows the reinforcement strains for P.F.S.1. The first yield strain was recorded by S.G.B at load 120 kN and S.G.A did not reach the yield strain. From Fig 6.(a) it seems that the strains are generally low in the bars.

Fig.6. (c) shows the reinforcement strains for P.F.S.2, strain gauge S.G.A and S.G.B did not reach yield strain. Even at failure S.G.A and S.G.B recorded small strains compared to the yield. Fig.6. (e) shows the reinforcement strains for P.F.S.6. The first yield strain was recorded by S.G.A at load 80 kN followed by S.G.B approximately at 100 kN. Even at crack load S.G.A and S.G.B recorded very small strains compared to the yield strain and then the strain increase. It seems from Fig 6. (e) that the strains were generally high at failure.

Fig .6.(g) shows the reinforcement strains for P.F.S.9. An electrical problem occurred for strain gauge S.G.B during test, and the strain gauge S.G.A did not reach the yield strain, and record very small strains during test.

Tendon Strains, Strains in the unbonded tendon was measured, at location as shown before in Fig.2, the profiles of the measured strains with loading are plotted in Fig 7. (b, d, f, h)

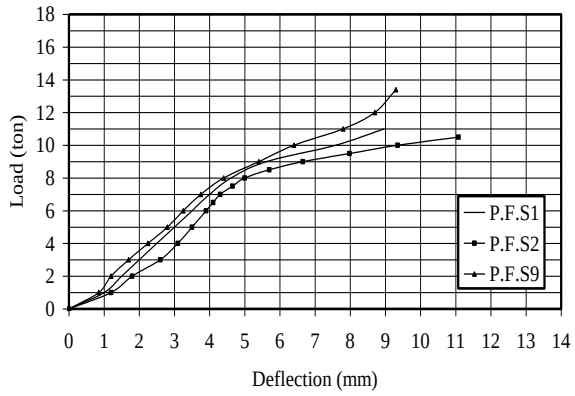

Fig.5. (a): Effect of Cables Number.

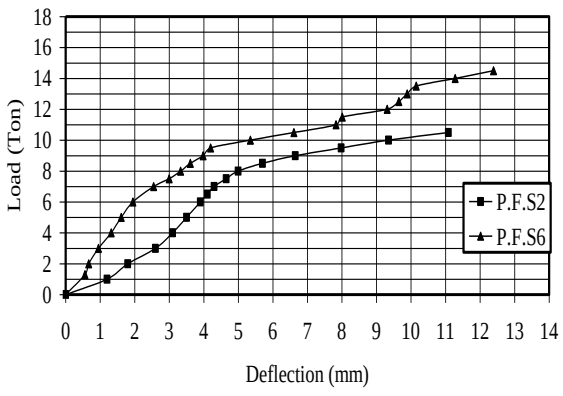

Fig.5. (b): Effect of Prestressing Force

International Journal of Sustainability and Innovation in Engineering
(IJSIE)
https://www.doi.org/10.56830/IJSIE062023

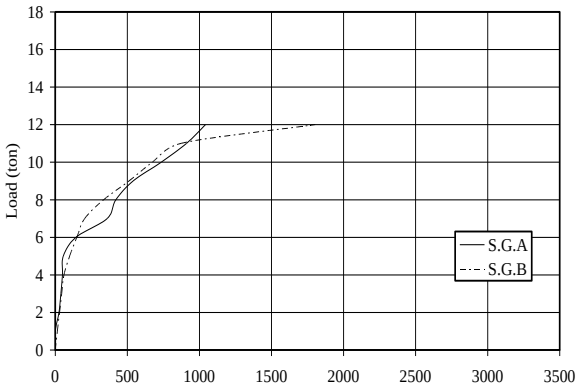

Strain x 10^{-6} (Steel strain)

Fig.6. (a): Load strain curve for P.F.S.1

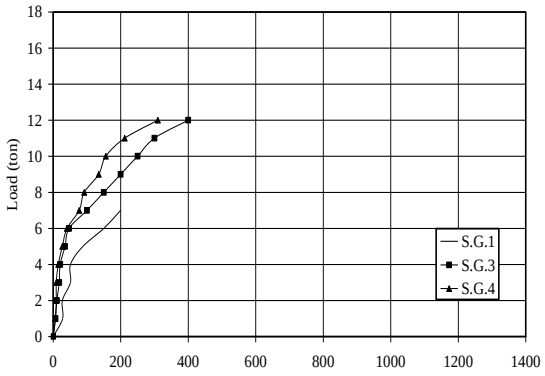

Strain x 10^{-6} (Strand strain)

Fig.6. (b): Load strain curve for P.F.S.1

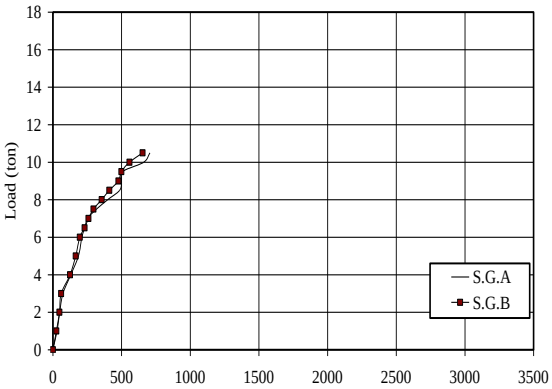

Strain x 10^{-6} (Steel strain)

Fig.6. (c): Load strain curve for P.F.S.2

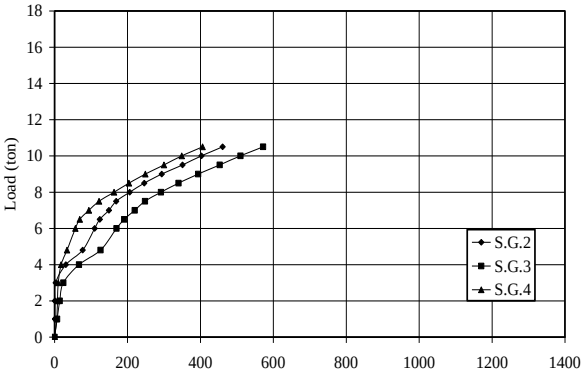

Strain x 10^{-6} (Strand strain)

Fig.6. (d): Load strain curve for P.F.S.2

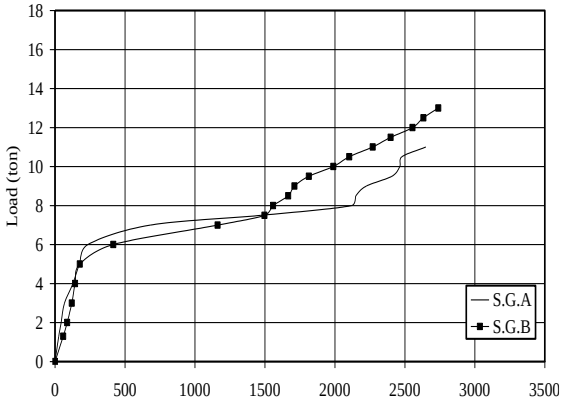

Strain x 10^{-6} (Steel strain)

Fig.6. (e): Load strain curve for P.F.S.6 slab

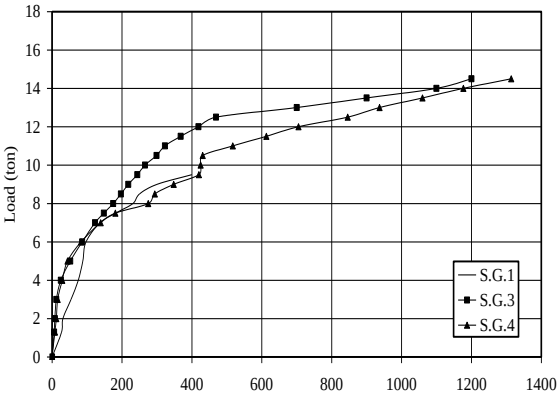

Strain x 10^{-6} (Strand strain)

Fig.6. (f): Load strain curve for P.F.S.6

International Journal of Sustainability and Innovation in Engineering
(IJSIE)
https://www.doi.org/10.56830/IJSIE062023

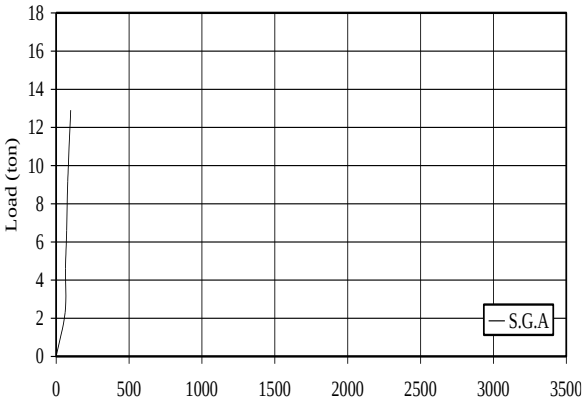

Strain x 10^{-6} (Steel strain)

Fig.6. (g): Load strain curve for P.F.S.9

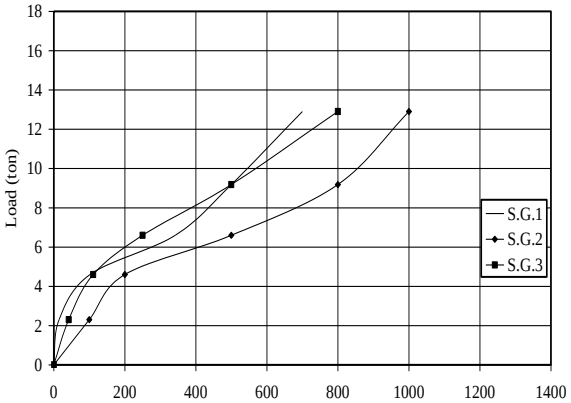

Strain x 10^{-6} (Strand strain)

Fig.6. (h): Load strain curve for P.F.S.9

Table 2: Results of slab tests.

Group No	Slab No	P_{cr} At first crack (kN)	P_f Failure load (kN)	Δ_{cr} (mm)	Δ_{so} (mm)	Δ_s (mm)	Δ_{max} (mm)	Rigidity (P_{cr}/Δ_{cr})
1	P.F.S1	56.00	124.0	3.35	5.20	5.20	8.97	1.67
	P.F.S2	51.00	110.0	3.60	5.70	4.70	11.08	1.42
	P.F.S9	56.00	134.0	3.50	4.75	5.70	9.30	1.60
2	P.F.S2	51.00	110.0	3.60	5.70	4.70	11.08	1.42
	P.F.S6	60.00	146.0	1.95	3.70	5.90	12.39	3.07

7.2 Comparison between Experimental Results and Different Codes.

Table 3.a: Comparison between Failure and Predicted Shear Force of slabs of group (1)

Slab No	$V_{(test)}$ kN	ACI 318 Test/Code	BS 8110 Test/Code	Gardner Test/Code
P.F.S.1	124	1.26	1.18	1.21
P.F.S.2	110	1.07	1.02	1.01
P.F.S.9	134	1.29	1.23	1.26
Average		1.21	1.14	1.16

Table 3.b: Comparison between Failure and Predicted Shear Force of slabs of group (2)

Slab No	$V_{(test)}$ kN	ACI 318 Test/Code	BS 8110 Test/Code	Gardner Test/Code
P.F.S.2	110	1.07	1.02	1.01
P.F.S.6	146	1.47	1.41	1.33
Average		1.27	1.22	1.17

7.2.1 Comparison with respect to the Number of Cables.

The American Code ACI 318-02

For P.F.S.1, P.F.S.2 and P.F.S.9 (represents the effect of the number of cables), the ratios (V_{test}/V_{code}) are 1.26, 1.07 and 1.29 respectively. It seems like the code is conservative for slabs P.F.S.1 and P.F.S.9. Table 3.a shows the relationship between the number of cables and the ratios (V_{test}/V_{code}). Such conservatism is clearly evident.

For P.F.S.2 ratios (V_{test}/V_{code}) it is less conservative because no tendon pass through the column, the ACI provision state that it must be two tendons passing through the column in two directions.

The British standard (BS 8110-97)

For P.F.S.1, P.F.S.2 and P.F.S.9 (represents the effect of the number of cables), the ratios (V_{test}/V_{code}) are 1.18, 1.02 and 1.23 respectively. It seems like the code is conservative for slabs P.F.S.1 and P.F.S.9. Table 3.a shows the relationship between the number of cables and the ratios (V_{test}/V_{code}). Such conservatism is clearly evident.The degree of conservatism increase with increasing number of cables.

Gardner method

For P.F.S.1, P.F.S.2 and P.F.S.9 (represents the effect of the number of cables), the ratios (V_{test}/V_{code}) are 1.21, 1.01 and 1.26 respectively. It seems like the code is conservative for slabs P.F.S.1 and P.F.S.9.

7.2.2 Comparison with respect to the Prestressing Force.

The American Code ACI 318-02

For P.F.S.2 and P.F.S.6 (represents the effect of the Prestressing Force), the ratios (V_{test}/V_{code}) are 1.07 and 1.47 respectively. It seems like the code is conservative for slabs P.F.S.1 and P.F.S.6.

The degree of conservatism increase with increasing the total prestressing force, the punching shear provisions of ACI 318-02 for slabs with only precompression or precompression and bonded reinforcement, even ignoring the vertical component of the prestressing force are significantly less conservative than those for reinforced concrete slabs.

The British standard (BS 8110-97)

For P.F.S.2 and P.F.S.6 the ratios (V_{test}/V_{code}) are 1.02 and 1.41 respectively. It seems like the code is conservative for slabs P.F.S.6 Table 3.b shows the

relationship between the number of cables and the ratios (V_{test}/V_{code}). Such conservatism is clearly evident, the degree of conservatism increase with increasing the prestressing force.

Gardner's method

For P.F.S.2 and P.F.S.6 the ratios (V_{test}/V_{code}) are 1.01 and 1.33 respectively. It seems like the code is conservative for slabs P.F.S.6. Table 3.b shows the relationship between the Total Prestressing Force and the ratios (V_{test}/V_{code}). Such conservatism is clearly evident. The degree of conservatism increase with increasing the prestressing force, in other words the provisions of the proposed method underestimate the effect of prestressing force.

8. CONCLUSION

Based on the analysis of experimental test results, the following conclusion can be drawn:

1- The flexural behaviour of post-tensioned concrete flat slabs in flexure is excellent with the slabs sustaining large loads before wide spread cracking takes place. Cracks are restricted to areas of high moment. However, the ultimate load capacity can be governed by punching shear failure.

2- Neglecting the vertical component of the prestressing force in calculations attributed to ACI 318-95, BS 8110-97 and the proposed method, will be conservative.

3- The punching shear provisions of ACI 318-02 for slabs with only precompression or precompression and bonded reinforcement, even ignoring the vertical component of the prestressing force are significantly less conservative than those for reinforced concrete slabs.

4- As many tendons in each direction as practical should pass through the column, with increasing number of tendons, an increases in the failure, crack load and improvement in the physical behavior of slabs.

5- Increasing the prestressing force lead to more confinement for slabs, and more enhancements in behavior and the punching shear capacity.

6- Increasing the prestressing force lead to an increase in the punching shear capacity of P.F.S.1 approximately by 32%.

9. REFERENCES:

ACI, C. (1989). Building Code Requirements for Reinforced Concrete (ACI 318-02) and Commentary—ACI 318 R-89. *American Con¬crete Institute, Farmington Hills*, pp. 353 .

ACI-ASCE, C. 4. (1989). "Recommendations for Concrete Members Prestressed With Unbonded Tendons". *ACI Structural Journal, V. 86, No. 3*, pp.301-318.

BS, 8. (1997, London). Structural Use of Concrete, Part 1 and Part 2, Code of Practice for Design and Construction. *British-Standard Institution*.

CEB-FIP. (1990). Model Code for Concrete, comite Euro-International du Beton and Federation International de la Precontrainte, Paris.

Gardner, N. J. (1996). "Punching Shear Provisions for Reinforced and Pre¬stressed Concrete Flat Slbs," . *CSCE Journal, V. 23, No 2*, pp. 502-510.

Shehata, I. A. (1990). "Simplified Model for Estimating the Punching Resistance of Reinforced Concrete Slabs,". *Materials and Struc-lures/Materiaux et Constructions, 23*, pp. 364-371.

Shehata, I. A., & Regan, P. E. (1989). "Punching in R.C. Slabs,". *Journal of Structural Engineering, ASCE, V. 115, No. 7*, pp. 1726-1740.

Shehata, I. A., & Shehata Lidia, C. D. (1989). "Compressive Strength of Concrete Elements with Variable Dimensions,". *Materials and, Structures. V. 22, No. 137*, pp. 264-268.